*J. Fluid Mech.* (2007), *vol.* 577, *pp.* 385–415.  
doi:10.1017/S002211200700479X Printed in the United Kingdom

# Segregation of a liquid mixture by a radially oscillating bubble

OLIVIER LOUISNARD[1], FRANCISCO J. GOMEZ[2] AND ROMAIN GROSSIER[1]

[1]Laboratoire de Génie des Procédés des Solides Divisés, Ecole des Mines d'Albi, 81013 Albi Cedex 09, France

[2]Laboratorio de Ultrasonidos, Dpto. de Fisica, Universidad de Santiago de Chile, Casilia 302, Santiago, Chile

(Received 15 December 2005 and in revised form 29 October 2006)

A theoretical formulation is proposed for forced mass transport by pressure gradients in a liquid binary mixture around a spherical bubble undergoing volume oscillations in a sound field. Assuming the impermeability of the bubble wall to both species, diffusion driven by pressure gradients and classical Fick-diffusion must cancel at the bubble wall, so that an oscillatory concentration gradient arises in the vicinity of the bubble. The Péclet number $Pe$ is generally high in typical situations and Fick diffusion cannot restore equilibrium immediately, so that an asymptotic average concentration profile may progressively build up in the liquid over large times. Such a behaviour is reminiscent of the so-called rectified diffusion problem, leading to slow growth of a gas bubble oscillating in a sound field. A rigorous method formerly proposed by Fyrillas & Szeri (*J. Fluid Mech.* vol. 277, 1994, p. 381) to solve the latter problem is used to solve the present one. It is based on splitting the problem into a smooth part and an oscillatory part. The smooth part is solved by a multiple scales method and yields the slowly varying average concentration field everywhere in the liquid. The oscillatory part is obtained by matched asymptotic expansions in terms of the small parameter $Pe^{-1/2}$: the inner solution is required to satisfy the oscillatory balance between pressure diffusion and Fick diffusion at the bubble wall, while the outer solution is required to be zero. Matching both solutions yields a unique splitting of the problem. The final analytical solution, truncated to leading order, compares successfully to direct numerical simulation of the full convection–diffusion equation. The analytical expressions for both smooth and oscillatory parts are calculated for various sets of bubble parameters: driving pressure, frequency and ambient radius. The smooth problem always yields an average depletion of the heaviest species at the bubble wall, only noticeable for large molecules or nano-particles. For driving pressures sufficiently high to yield inertial oscillations of the bubble, the oscillatory problem predicts a periodic peak excess concentration of the heaviest species at the bubble wall at each collapse, lingering on several tens of the time of the characteristic duration of the bubble rebound. The two effects may compete for large molecules and practical implications of this segregation phenomenon are proposed for various processes involving acoustic cavitation.

## 1. Introduction

Radially oscillating bubbles forced by a sound field are commonly encountered in acoustic cavitation and sonoluminescence experiments (Crum *et al.* 1999). Generally,

the liquid surrounding such bubbles is not pure and involves various chemical species, which may either participate in chemical reactions, or undergo phase transitions, such as crystallization processes. The kinetics of such processes depends on the concentrations of the species and may therefore be influenced by any variation of the spatial homogeneity of the mixture.

Pressure gradients may be a possible source of mixture segregation. Following diffusion theory (Bird, Stewart & Lightfoot 1960; Hirschfelder, Curtiss & Bird 1967), when a mixture of two species is subjected to a pressure gradient, the lighter one is pushed toward low-pressure regions. This forced diffusion process, known as pressure diffusion, generally remains weak unless the liquid is submitted to high-pressure gradients, as in ultracentrifuge applications where it is used profitably to separate large molecular weight species from a solvent (Archibald 1938). Pressure diffusion is also responsible for gas stratification in a quiescent atmosphere, or solute–solvent segregation in long sedimentation columns (Mullin & Leci 1969; Larson & Garside 1986). Besides, the effect of pressure diffusion, along with thermal diffusion, on the segregation of a gas mixture inside a radially oscillating bubble has been investigated by Storey & Szeri (1999) in the context of sonoluminescence.

When a bubble is driven in radial motion by a high-amplitude oscillating pressure field, pressure gradients arise in the liquid, as a result of the bubble wall acceleration. Inertial cavitation is a situation where the bubble suffers an explosive expansion followed by a violent collapse. In this case, the pressure gradient reaches a very high value near the end of the collapse, owing to the strong gas compression in the bubble. The segregation of two species by pressure diffusion in the neighbourhood of a cavitation bubble may therefore notably influence the liquid homogeneity.

The similar problem of mass transport of a gas dissolved in a liquid around a bubble undergoing volume oscillations has been studied extensively (Hsieh & Plesset 1961; Eller & Flynn 1965; Fyrillas & Szeri 1994, 1995): the variations of the gas concentration at the bubble wall, driven by the bubble oscillations, yield a non-zero average gas flux toward the bubble, reversing its natural dissolution process, a phenomenon known as rectified diffusion. In this case, the dissolved gas flux in the liquid arises as a consequence of the asymmetry in the behaviour of the two components at the bubble wall: the gas can cross the interface, the liquid cannot. In the present problem, assuming a binary mixture of two non-volatile and non-surface-active fluids, the bubble interface acts as a barrier for the two species, which would prohibit any relative flux. However, if pressure diffusion is taken into account, a new asymmetry between the two components arises, owing to their different densities, and the pressure gradient near the bubble wall separates the two species. Since the net flux across the bubble wall of any of the two species must be zero, a non-zero Fick diffusion flux must exactly balance the pressure diffusion flux. Thus, a concentration gradient should appear near the bubble wall and by continuity in the whole liquid. Since the pressure gradient reverses as the bubble oscillates, it is clear that the concentration of each species is an oscillatory quantity, but the question also arises of a possible average effect, building over several periods, as observed for rectified diffusion.

In the present paper, an approximate analytical expression of the concentration field in the liquid is sought in order to be able to draw some conclusions for a given mixture and given bubble parameters, namely the amplitude of the driving pressure, its frequency and the ambient radius of the bubble. Since the problem has some common characteristics with rectified diffusion, the solution method proposed by Fyrillas & Szeri (1994) will be used. The concentration field is cut into two parts: the

oscillating field is required to fulfil the complicated oscillatory part of the boundary condition at the bubble wall and is non-zero only in a thin boundary layer near the bubble; the smooth field satisfies the remaining part of the boundary condition and is uniformly valid everywhere in the liquid. No specific assumption is made concerning bubble dynamics, apart from its periodic motion, so that the solution obtained is immediately applicable once the bubble radius is known as a function of time.

The paper is organized as follows: § 2 presents the main convection–diffusion equation along with boundary conditions and the splitting of the problem in two parts. In § 3, the oscillatory problem is solved and the splitting is determined unambiguously. The smooth problem is solved in § 4. In § 5, the analytical results are first validated by comparing them to a full numerical solution of the partial differential equation, then, the influence of the bubble parameters on the magnitude of the segregation effect is investigated. In § 6, the model is finally applied to typical mixtures of water with either small or large molecules, and the results are discussed.

## 2. Formulation

### 2.1. *Bubble motion and liquid fields*

We will consider a single bubble oscillating in a liquid mixture of infinite extent, forced by a oscillating pressure field far from the bubble $p_\infty(t) = p_0(1 - P\cos\omega t)$, where $\omega$ is the angular frequency, $P$ the dimensionless forcing pressure and $p_0$ the hydrostatic pressure. The motion of such a bubble has been widely described in the literature since the early work of Lord Rayleigh and several refinements of the basic model can be found, including thermal behaviour of the gas, liquid compressibility effects and liquid evaporation at the bubble wall (see Prosperetti 1999; Brenner, Hilgenfeldt & Lohse 2002, for a recent review).

The model presented here is in itself independent of the specific bubble dynamics model, and we defer the choice of the differential equation governing the radial motion to § 5. However, the mass transport equation used in this work requires analytical expressions of the velocity and pressure fields in the liquid, and for the sake of simplicity, we will assume an iso-volume motion of the liquid. Besides, the potential character of the flow is ensured by the spherical symmetry, and the potential $\tilde{\phi}$ and velocity fields $\tilde{v}$ can be easily obtained from mass conservation:

$$\tilde{\phi}(r,t) = -\frac{1}{4\pi r}\frac{\mathrm{d}\tilde{V}}{\mathrm{d}t}, \tag{2.1}$$

$$\tilde{\boldsymbol{v}}(r,t) = \frac{\boldsymbol{r}}{4\pi r^3}\frac{\mathrm{d}\tilde{V}}{\mathrm{d}t}, \tag{2.2}$$

where $\tilde{V}$ is the time-dependent bubble volume, and $r$ the distance from the centre of the bubble. Then, using the unsteady Bernoulli law for potential flows between a point in the liquid of radial coordinate $r$ and a point infinitely far from the bubble, the pressure field in the liquid is

$$\tilde{p}(r,t) = p_\infty(t) + \rho\left[\frac{1}{4\pi r}\frac{\mathrm{d}^2\tilde{V}}{\mathrm{d}t^2} - \frac{1}{32\pi^2 r^4}\left(\frac{\mathrm{d}\tilde{V}}{\mathrm{d}t}\right)^2\right]. \tag{2.3}$$

The validity of the iso-volume assumption is questionable for strong motion of the bubble, involving wall velocities near to or greater than the speed of sound in the liquid. Accounting for liquid compressibility results in corrections of the order of the Mach number in both the velocity and pressure field, and therefore also in the

bubble dynamics equation (Prosperetti & Lezzi 1986). The main physical consequence of liquid compressibility is the formation of shock-waves at the end of the bubble collapse (Hickling & Plesset 1964). Clearly, since shock-waves are in essence strong pressure gradients, neglecting their effect on pressure diffusion may appear as a rough approximation. However, taking them into account would require cumbersome expressions of the velocity and pressure fields (see for example, the second-order expressions of Tomita & Shima 1977; Fujikawa & Akamatsu 1980, obtained by the PLK strained-coordinates method). This constitutes a technical problem, especially for the velocity field: as will be seen below, the convective term in the transport equation can easily be suppressed by a convenient change of variable in the incompressible case. There is no evidence that a similar change of variable could be found in the case of a compressible velocity field, which would make the problem untractable. We therefore chose to sacrifice the compressibility hypothesis in order to draw a general picture of the pressure diffusion effect. We will, however, make an exception and keep the compressibility-induced correction terms in the bubble equation, in order to obtain a more realistic model for the bubble dynamics. Moreover, since the shock-waves issue is of practical interest, additional qualitative comments will be proposed in § 6.

Finally, since the liquid considered here is a mixture whose spatial homogeneity is investigated, the average mixture density may not be constant. It may reasonably be assumed that the occurrence of such inhomogeneities significantly affects neither the liquid fields, nor the bubble motion.

### 2.2. *Mass transport*

The mass conservation of a species A in a binary mixture is expressed as

$$\frac{\partial \rho_A}{\partial t} + \nabla \cdot (\rho_A \tilde{\boldsymbol{v}}) = -\nabla \cdot \boldsymbol{j}_A, \tag{2.4}$$

where $\rho_A$ is the local density of species A, $\tilde{\boldsymbol{v}}$ is the mass-averaged mixture velocity. The mass diffusion flux $\boldsymbol{j}_A$ is, taking into account pressure diffusion (Bird *et al.* 1960; Hirschfelder *et al.* 1967)

$$\boldsymbol{j}_A = -D\left[\rho \nabla \omega_A + \frac{M_A M_B}{M \mathscr{R} T} \rho \omega_A \left(\frac{\bar{V}_A}{M_A} - \frac{1}{\rho}\right) \nabla \tilde{p}\right], \tag{2.5}$$

where $\omega_A = \rho_A/\rho$ is the mass fraction of species A, $M_A$, $M_B$ and $M$ are the respective molar weight of species A, B and of the mixture, $\rho$ is the mean density of the mixture, $\bar{V}_A$ the specific molal volume of species A, and $\mathscr{R}$ the universal gas constant. The first term in (2.5) represents the Fick diffusion flux, driven by a concentration gradient, and the second is the pressure diffusion flux, driven by the local pressure gradient.

Using the mixture mass-conservation equation $\partial \rho/\partial t + \nabla \cdot (\rho \tilde{\boldsymbol{v}}) = 0$, and inserting the flux expression (2.5) in (2.4), we obtain:

$$\rho\left(\frac{\partial \omega_A}{\partial t} + \tilde{\boldsymbol{v}} \cdot \nabla \omega_A\right) = D \nabla \cdot \left\{\rho\left[\nabla \omega_A + \frac{M_A M_B}{M \mathscr{R} T} \omega_A \left(\frac{\bar{V}_A}{M_A} - \frac{1}{\rho}\right) \nabla \tilde{p}\right]\right\}. \tag{2.6}$$

Although it is tempting to simplify both sides of (2.6) by $\rho$, the latter quantity is not constant since it depends on the local mass fraction $\omega_A$, which is space and time dependent. The same problem arises with the appearance of the mean molar weight $M$ and again the density $\rho$ in the pressure diffusion term of (2.6), which depends on the local composition of the mixture. This has the strong consequence that rigorously, (2.6) is nonlinear. In view of the method we plan to use for the resolution of the problem, a linearization of the problem is necessary, paying the price

of some additional assumptions. It is shown in Appendix A that in the limit of a dilute mixture ($\omega_A \ll 1$), the mixture density $\rho$ is approximately constant and equal to $M_B/\bar{V}_B$ and (2.6) may be simplified as

$$\frac{\partial \omega_A}{\partial t} + \tilde{\boldsymbol{v}} \cdot \nabla \omega_A = D \nabla \cdot \left[ \nabla \omega_A + \frac{M_A}{\mathscr{R}T} \omega_A \left( \frac{\bar{V}_A}{M_A} - \frac{\bar{V}_B}{M_B} \right) \nabla \tilde{p} \right], \tag{2.7}$$

or, in spherical coordinates:

$$\frac{\partial \omega_A}{\partial t} + \tilde{v}(r,t) \frac{\partial \omega_A}{\partial r} = \frac{D}{r^2} \frac{\partial}{\partial r} \left[ r^2 \left( \frac{\partial \omega_A}{\partial r} + \tilde{\beta} \omega_A \frac{\partial \tilde{p}}{\partial r}(r,t) \right) \right], \tag{2.8}$$

where $\tilde{v}(r,t)$ and $\tilde{p}(r,t)$ are given by (2.2) and (2.3), and $\tilde{\beta}$ is:

$$\tilde{\beta} = \frac{M_A}{\mathscr{R}T} \left( \frac{\bar{V}_A}{M_A} - \frac{\bar{V}_B}{M_B} \right). \tag{2.9}$$

This conservation equation should be completed with appropriate boundary conditions at the bubble wall and infinitely far from the bubble. Both components are assumed non-volatile and therefore cannot cross the bubble wall. Thus, the diffusive flux $\boldsymbol{j}_A$ should be zero at the bubble wall:

$$\frac{\partial \omega_A}{\partial r}(r = \tilde{R}(t), t) + \tilde{\beta} \omega_A (r = \tilde{R}(t), t) \frac{\partial \tilde{p}}{\partial r}(r = \tilde{R}(t), t) = 0. \tag{2.10}$$

We emphasize that the expression of the diffusive flux at the bubble wall must include the pressure diffusion term, consistently with the transport equation, (2.8). A similar boundary condition is used in centrifuge equations (Archibald 1938), to express the impermeability of the sample-tube extremities to any species. The non-volatility of the species may appear as a drastic limitation. However, relaxing this hypothesis would have the disadvantage of coupling the diffusion problem in the liquid with the diffusion problem of vapour through the uncondensable gas filling the bubble. Moreover, the problem would require a liquid–vapour equilibrium condition at the bubble wall, which may take a complex form in the case of mixtures. Finally, several related issues such as evaporation–condensation kinetics, or chemical reactions (Storey & Szeri 2000) may further complicate the problem. We therefore leave aside these refinements for now, and concentrate on the effects of pressure diffusion alone.

Far from the bubble, the concentration field remains undisturbed by the bubble oscillations, so that

$$\omega_A(r \to \infty, t) = \omega_{A0}, \tag{2.11}$$

and finally, the liquid mixture is initially assumed homogeneous in space:

$$\omega_A(r, t = 0) = \omega_{A0}. \tag{2.12}$$

### 2.3. *Non-dimensionalization*

The equations of the problems are non-dimensionalized as follows: the natural length scale is the ambient bubble radius $\tilde{R}_0$, the time scale is $\omega^{-1}$, the inverse of the driving frequency. The pressure scale is set as $\rho_0 \tilde{R}_0^2 \omega^2/2$, which is the dynamic pressure of the liquid displaced by the bubble. We therefore set

$$r = \tilde{R}_0 \xi, \quad t = \tau/\omega, \quad \tilde{p} = \tfrac{1}{2} \rho \tilde{R}_0^2 \omega^2 p.$$

The bubble instantaneous radius and volume are non-dimensionalized by their ambient values:

$$\tilde{R} = \tilde{R}_0 R, \quad \tilde{V} = \tfrac{4}{3} \pi \tilde{R}_0^3 V.$$

In the new variables, the dimensionless velocity and pressure field in the liquid are

$$v(\xi, \tau) = \frac{\dot{V}}{3\xi}, \tag{2.13a}$$

$$p(\xi, \tau) = \frac{2}{3}\frac{\ddot{V}}{\xi} - \frac{1}{9}\frac{\dot{V}^2}{\xi^4}, \tag{2.13b}$$

where here, and in what follows, overdots denote time derivatives with respect to the dimensionless time variable $\tau$. The concentration of species A is non-dimensionalized by

$$C = \frac{\omega_A}{\omega_{A0}} - 1. \tag{2.14}$$

The quantity $C$ represents the segregation level: a positive value of $C$ expresses a local excess of species A above the concentration at rest. The mass transport equation becomes

$$\frac{\partial C}{\partial \tau} + \left(\frac{\dot{V}}{3\xi^2}\right)\frac{\partial C}{\partial \xi} = \frac{1}{Pe}\frac{1}{\xi^2}\frac{\partial}{\partial \xi}\left\{\xi^2\left[\frac{\partial C}{\partial \xi} + \beta(C+1)\frac{\partial p}{\partial \xi}\right]\right\}, \tag{2.15}$$

where $Pe = \tilde{R}_0^2\omega/D$ is the Péclet number, and the dimensionless number $\beta$ is

$$\beta = \tilde{\beta}\tfrac{1}{2}\rho\tilde{R}_0^2\omega^2. \tag{2.16}$$

For later use, we separate the respective contributions of the mixture and the bubble to the dimensionless parameter $\beta$, and write

$$\beta = \beta_m\tilde{R}_0^2\omega^2, \tag{2.17}$$

where

$$\beta_m = \tfrac{1}{2}\tilde{\beta}\rho = \frac{1}{2}\frac{M_A}{\mathscr{R}T}\left(\frac{\bar{V}_A}{M_A}\frac{M_B}{\bar{V}_B} - 1\right), \tag{2.18}$$

depends only on the mixture considered.

The boundary and initial conditions become, in dimensionless variables

$$\frac{\partial C}{\partial \xi}(\xi = R(\tau), \tau) + \beta[C(\xi = R(\tau), \tau) + 1]\frac{\partial p}{\partial \xi}(\xi = R(\tau), \tau) = 0, \tag{2.19a}$$

$$C(\xi \to \infty, \tau) = 0, \tag{2.19b}$$

$$C(\xi, \tau = 0) = 0. \tag{2.19c}$$

The intrinsic difficulties in the resolution of the above governing equations are similar to those encountered in the rectified diffusion problem (Hsieh & Plesset 1961; Eller & Flynn 1965; Fyrillas & Szeri 1994, 1995): on one hand, the boundary condition (2.19*a*) at the bubble surface is applied at a moving boundary and is furthermore unsteady. On the other hand, the velocity field is inhomogeneous and also unsteady. The solution to overcome the difficulty of the moving boundary and the oscillating velocity field is to define a Lagrangian radial coordinate, as first suggested by Plesset & Zwick (1952), by $\sigma = (\xi^3 - V(\tau))/3$, which represents physically the dimensionless volume between the bubble wall and the point of interest in the liquid. A specific liquid particle moves with a constant $\sigma$ (under the incompressibility hypothesis) and an observer moving with such a particle would see only the diffusive transport of species. This may be readily seen by expressing (2.15) in the Lagrangian coordinates

$(\sigma, \tau)$:

$$\frac{\partial C}{\partial \tau} = \frac{1}{Pe}\frac{\partial}{\partial \sigma}\left[A(\sigma, \tau)\frac{\partial C}{\partial \sigma} + \beta B(\sigma, \tau)(C+1)\right], \tag{2.20}$$

where

$$A(\sigma, \tau) = (3\sigma + V)^{4/3}, \tag{2.21a}$$

$$B(\sigma, \tau) = -\frac{2}{3}\ddot{V} + \frac{4}{9}\frac{\dot{V}^2}{(3\sigma + V)}. \tag{2.21b}$$

The boundary and initial conditions (2.19) become

$$\frac{\partial C}{\partial \sigma}(0, \tau) + \beta\frac{B(0, \tau)}{A(0, \tau)}(C(0, \tau) + 1) = 0, \tag{2.22a}$$

$$C(\sigma \to \infty, \tau) = 0, \tag{2.22b}$$

$$C(\sigma, \tau = 0) = 0. \tag{2.22c}$$

It can readily be seen that the convective term of (2.15) has indeed disappeared and that the boundary condition at the bubble wall is now applied at a fixed point, thanks to the change of variable.

The problem defined by (2.20)–(2.22) shows some resemblance to the rectified diffusion problem and thus, the splitting-method proposed by Fyrillas & Szeri (1994, 1995, 1996) can profitably be used here. For self-completeness, we will recall here the main lines of its underlying physical basis. For rectified diffusion, the oscillatory gas pressure in the bubble drives the gas concentration in the neighbouring liquid in oscillation, thus producing a periodic inversion of the concentration gradient. This rapidly oscillating gradient is counteracted by molecular diffusion, but owing to the large value of the Péclet number, the equilibrium cannot be restored immediately. This delay produces a long-term average diffusion effect, on a time scale larger than the oscillation period by a factor of the order of $Pe$. Therefore, the concentration field varies on two time-scales.

The present problem shares this property with rectified diffusion, but here, the source of the concentration gradient is the segregation of species by pressure diffusion, both in the liquid bulk and at the bubble wall (see (2.20) and (2.22*a*), respectively). Moreover, it can easily be seen by looking at (2.13*b*) or (2.21*b*) that pressure diffusion is not symmetric over one oscillation period, owing to the $\dot{V}^2$ term, representing the convective acceleration of the fluid in spherical symmetry. Because of this term, pressure increases when travelling away from the bubble, which may be understood from the Bernoulli law: because of spherical symmetry, velocity decreases with the distance to the bubble and this should be balanced by a pressure increase.

For both rectified diffusion and the present problem, the existence of two time scales justifies a multiple-scales method, but there remains a technical difficulty in the unsteady character of the boundary conditions at the bubble wall. If the multiple-scales method were to be applied directly to the set of equations (2.20), (2.22), one would be met with the impossibility for the solution at leading order to fulfil the oscillating boundary condition (2.22*a*). This difficulty is overcome by splitting the concentration field into two parts: an oscillatory part, which satisfies the oscillating part of the boundary condition, and a smooth part, to which the remaining part of the boundary condition should be ascribed. The oscillating part represents physically the perturbation of the concentration field imposed by the bubble wall forcing term, and is designed to differ from zero only in a boundary layer of thickness $Pe^{-1/2}$. The

smooth part extends in the whole liquid and varies on both the oscillation time scale $1/\omega$ and a slow time scale of order $Pe/\omega$.

### 2.4. *Splitting of the problem*

We set the concentration field as $C(\sigma,\tau)=C^{osc}(\sigma,\tau)+C^{sm}(\sigma,\tau)$, where $C^{osc}$ is the oscillatory part, and $C^{sm}$ the smooth part. We then split the governing equations into an oscillatory part and a smooth part. The oscillatory problem is defined by

$$\frac{\partial C^{osc}}{\partial\tau}=\frac{1}{Pe}\frac{\partial}{\partial\sigma}\left[A(\sigma,\tau)\frac{\partial C^{osc}}{\partial\sigma}+\beta B(\sigma,\tau)C^{osc}\right], \tag{2.23a}$$

$$\frac{\partial C^{osc}}{\partial\sigma}(0,\tau)+\beta H(\tau)[C^{osc}(0,\tau)+1]=-G-\beta H(\tau)C^{sm}(0,\tau), \tag{2.23b}$$

and the smooth problem is

$$\frac{\partial C^{sm}}{\partial\tau}=\frac{1}{Pe}\frac{\partial}{\partial\sigma}\left[A(\sigma,\tau)\frac{\partial C^{sm}}{\partial\sigma}+\beta B(\sigma,\tau)(C^{sm}+1)\right], \tag{2.24a}$$

$$\frac{\partial C^{sm}}{\partial\sigma}(0,\tau)=G. \tag{2.24b}$$

The constant $G$ is introduced to add a degree of freedom in the separation process and will be determined unambiguously by using a splitting condition, to be defined in the next section. In the boundary condition (2.23*b*), the function $H(\tau)$ is defined by

$$H(\tau)=\frac{B(0,\tau)}{A(0,\tau)}, \tag{2.25}$$

and represents the dimensionless pressure gradient at the bubble wall.

Finally, both oscillatory and smooth fields are required to fulfil the boundary condition far from the bubble (2.22*b*) and the initial condition (2.22*c*), so that

$$C^{sm}(\sigma\to\infty,\tau)=C^{sm}(\sigma,0)=0, \tag{2.26}$$

$$C^{osc}(\sigma\to\infty,\tau)=C^{osc}(\sigma,0)=0. \tag{2.27}$$

## 3. The oscillatory problem

Following Fyrillas & Szeri (1995), we use a matched asymptotic expansion to solve the oscillatory problem: the inner solution must fulfil the bubble wall boundary condition (2.23*b*) while the outer solution is required to be identically zero. To determine the inner approximation of the oscillatory solution, we define a re-scaled Lagrangian space-coordinate by $s=Pe^{1/2}\sigma$. Furthermore, we use the nonlinear time $\hat{\tau}$ first suggested by Plesset & Zwick (1952), which arises from the spherical symmetry of the problem:

$$\hat{\tau}=\int_0^{\tau}R^4(\tau')\,\mathrm{d}\tau', \tag{3.1}$$

and for further use, we also define the nonlinear period

$$\hat{T}=\int_0^{2\pi}R^4(\tau')\,\mathrm{d}\tau'. \tag{3.2}$$

Taking $\hat{\tau}$ as the new time variable, (2.23*a*) becomes

$$\frac{\partial C^{osc}}{\partial\hat{\tau}}=\frac{\partial}{\partial s}\left[A'(s,\hat{\tau};Pe)\frac{\partial C^{osc}}{\partial s}+\frac{1}{Pe^{1/2}}\beta B'(s,\hat{\tau};Pe)C^{osc}\right], \tag{3.3}$$

where

$$A'(s,\hat{\tau};Pe) = R^{-4}A(Pe^{-1/2}s,\tau) = \left(1+\frac{1}{Pe^{1/2}}\frac{3s}{V}\right)^{4/3}, \tag{3.4a}$$

$$B'(s,\hat{\tau};Pe) = R^{-4}B(Pe^{-1/2}s,\tau) = -\frac{2}{3}\frac{\ddot{V}}{V^{4/3}} + \frac{4}{9}\frac{\dot{V}^2}{V^{7/3}}\frac{1}{1+\dfrac{1}{Pe^{1/2}}\dfrac{3s}{V}}, \tag{3.4b}$$

and the bubble wall condition reads

$$Pe^{1/2}\frac{\partial C^{osc}}{\partial s}(0,\hat{\tau}) + \beta H(\hat{\tau})\,[C^{osc}(0,\hat{\tau})+1] = -G - \beta H(\hat{\tau})C^{sm}(0,\hat{\tau}). \tag{3.5}$$

The outer limit of the inner approximation should match the outer approximation which is identically zero, so that $C^{osc}(s,\hat{\tau})$ should satisfy

$$\lim_{s\to\infty} C^{osc}(s,\hat{\tau}) = 0. \tag{3.6}$$

We now assume an asymptotic expansion for $C^{osc}$ in the $Pe^{-1/2}$ parameter:

$$C^{osc}(s,\hat{\tau}) = C_0^{osc}(s,\hat{\tau}) + \frac{1}{Pe^{1/2}}C_1^{osc}(s,\hat{\tau}) + \frac{1}{Pe}C_2^{osc}(s,\hat{\tau})\ldots, \tag{3.7}$$

and we also expand functions $A'$ and $B'$ given by (3.4), as well as the separation constant $G$ appearing in (2.23*b*) and(2.24):

$$A'(s,\hat{\tau}) = 1 + Pe^{-1/2}A_1'(s,\hat{\tau}) + Pe^{-1}A_2'(s,\hat{\tau})\ldots,$$
$$B'(s,\hat{\tau}) = B_0'(\hat{\tau}) + Pe^{-1/2}B_1'(s,\hat{\tau}) + Pe^{-1}B_2'(s,\hat{\tau})\ldots,$$
$$G = G_0 + Pe^{-1/2}G_1 + Pe^{-1}G_2\ldots.$$

A hierarchy of inhomogeneous diffusion problems is obtained, all sharing the same form. The general solution of such problems is detailed in Appendix B, which also yields a splitting-condition necessary to ensure the matching equation (3.6). In the present case, the oscillatory problem at each order has a Neumann boundary condition, whereas the oscillatory problems in the analysis of surfactant-enhanced rectified diffusion by Fyrillas & Szeri (1995) involve a Dirichlet boundary condition. The difference arises from the presence of the Péclet number in the boundary condition in the latter problem (see equation (2.4) in Fyrillas & Szeri 1995), whereas the boundary condition (2.22*a*) in the present problem is Péclet independent. This is because both pressure and Fick diffusion terms are proportional to the diffusion coefficient, which thus cancels out in the null total flux condition (2.10) at the bubble wall.

For further use, it is useful to note that the $H$ function given by (2.25) can also be expressed in the following forms

$$H(\hat{\tau}) = B_0'(\hat{\tau}) = -\frac{2}{3}\frac{\ddot{V}}{V^{4/3}} + \frac{4}{9}\frac{\dot{V}^2}{V^{7/3}} = -2\frac{\ddot{R}}{R^2}. \tag{3.8}$$

We now turn to solve the oscillatory problems at each order.

### 3.1. *Zeroth-order*

The oscillatory problem at order 0 is

$$\frac{\partial C_0^{osc}}{\partial\hat{\tau}} = \frac{\partial^2 C_0^{osc}}{\partial s^2}, \quad \frac{\partial C_0^{osc}}{\partial s}(0,\hat{\tau}) = 0, \quad C_0^{osc}(s\to\infty) = 0. \tag{3.9a–c}$$

The solution is clearly the null one. This can be easily understood on a physical basis as pressure diffusion does not act to this order, neither in the liquid bulk, nor at the bubble wall, as can be seen in (3.9*a–c*). Therefore the liquid mixture is submitted only to classical molecular diffusion. Only a non-homogeneous boundary condition could produce a concentration gradient which is not the case, since to this order, the bubble wall condition imposes only a zero concentration gradient. This is why, contrarily to rectified diffusion problems (Fyrillas & Szeri 1994, 1995), the zeroth-order oscillatory solution is zero in the present problem.

### 3.2. *First-order*

At order 1, using the nullity of $C_0^{osc}(0,\hat{\tau})$, we obtain:

$$\frac{\partial C_1^{osc}}{\partial \hat{\tau}} = \frac{\partial^2 C_1^{osc}}{\partial s^2}, \tag{3.10a}$$

$$\frac{\partial C_1^{osc}}{\partial s}(0,\hat{\tau}) + \beta H(\hat{\tau}) = -G_0 - \beta H(\hat{\tau}) C_0^{sm}(0,\hat{\tau}), \tag{3.10b}$$

$$C_1^{osc}(s \to \infty) = 0. \tag{3.10c}$$

The splitting-condition (B 7) obtained in Appendix B yields the separation constant $G_0$:

$$G_0 = -\beta \left\langle H(\hat{\tau}) \left[ C_0^{sm}(0,\tau) + 1 \right] \right\rangle_{\hat{\tau}}. \tag{3.11}$$

The part of the boundary condition ascribed to $C_1^{osc}$ is therefore

$$\frac{\partial C_1^{osc}}{\partial s}(0,\hat{\tau}) = \beta \left[ \langle H(\hat{\tau}) \rangle_{\hat{\tau}} - H(\hat{\tau}) \right] \left[ C_0^{sm}(0) + 1 \right],$$

where we have used the result, to be demonstrated in § 4, that $C_0^{sm}$ is independent of the fast time-variable $\hat{\tau}$. The asymptotic solution $\bar{C}_1^{osc}(s,\hat{\tau})$ of equations (3.10 *a–c*) can be obtained from Appendix B: expanding $H(\hat{\tau})$ as a Fourier series,

$$H(\hat{\tau}) = \langle H(\hat{\tau}) \rangle_{\hat{\tau}} + \sum_{\substack{m=-\infty \\ m\neq 0}}^{m=+\infty} h_m \exp\left( 2\mathrm{i}m\pi \frac{\hat{\tau}}{\hat{T}} \right), \tag{3.12}$$

and using (B 8), the oscillatory concentration field is

$$\bar{C}_1^{osc}(s,\hat{\tau}) = \beta \left[ C_0^{sm}(0) + 1 \right] \left( \frac{\hat{T}}{2\pi} \right)^{1/2} \times \sum_{\substack{m=-\infty \\ m\neq 0}}^{m=+\infty} \frac{h_m}{|m|^{1/2}} \exp\left[ \mathrm{i}\left( 2\pi m \frac{\hat{\tau}}{\hat{T}} - \epsilon_m \frac{\pi}{4} \right) - (\epsilon_m \mathrm{i} + 1) \left( \frac{|m|\pi}{\hat{T}} \right)^{1/2} s \right], \tag{3.13}$$

where $\epsilon_m = \mathrm{sgn}(m)$. The first-order oscillatory solution $\bar{C}_1^{osc}$ depends on the boundary value of the zeroth-order smooth solution $C_0^{sm}(0)$, which is to be determined in the next section.

### 3.3. *Second-order*

The second-order oscillatory problem allows the determination of the separation constant $G_1$, which, as will be seen below, is enough to solve the smooth problem up to order $Pe^{-1}$. The calculation is detailed in Appendix C and yields

$$G_1 = -\beta \left\langle H(\hat{\tau}) \left[ C_1^{sm}(0,\tau) \right] \right\rangle_{\hat{\tau}}. \tag{3.14}$$

The second-order oscillatory field $C_2^{osc}$ could also be obtained analytically by using Appendix B, but is not required in the present analysis.

## 4. The smooth problem

To treat the smooth problem, time is first rescaled by defining the slow time variable $\lambda = \tau/Pe$, and the smooth field $C^{sm}$ is considered as a function of both fast and slow time variables, respectively $\tau$ and $\lambda$. The smooth equation (2.24*a*) reads, in the new variables

$$\frac{\partial C^{sm}}{\partial \tau} + \frac{1}{Pe}\frac{\partial C^{sm}}{\partial \lambda} = \frac{1}{Pe}\frac{\partial}{\partial \sigma}\left[A(\sigma,\tau)\frac{\partial C^{sm}}{\partial \sigma} + \beta B(\sigma,\tau)(C^{sm}+1)\right]. \tag{4.1}$$

The smooth field $C^{sm}(\sigma,\tau,\lambda)$ is next expanded in the small parameter $Pe^{-1/2}$:

$$C^{sm}(\sigma,\tau,\lambda) = C_0^{sm}(\sigma,\tau,\lambda) + \frac{1}{Pe^{1/2}}C_1^{sm}(\sigma,\tau,\lambda) + \frac{1}{Pe}C_2^{sm}(\sigma,\tau,\lambda) + \ldots, \tag{4.2}$$

which, once introduced in (4.1), yields a hierarchy of equations in the small parameter $Pe^{-1/2}$. As in Fyrillas & Szeri (1995), the zeroth- and first-order smooth equations read simply:

$$\frac{\partial C_0^{sm}}{\partial \tau} = 0 \Rightarrow C_0^{sm}(\sigma,\lambda), \quad \frac{\partial C_1^{sm}}{\partial \tau} = 0 \Rightarrow C_1^{sm}(\sigma,\lambda), \tag{4.3a,b}$$

which indicates that $C_0^{sm}$ and $C_1^{sm}$ vary with time only through the slow time scale $\lambda$. The dependence of these two fields on $\sigma$ and $\lambda$ can be obtained by writing the problems at orders 2 and 3, and using a non-secularity condition. The smooth boundary condition (2.24*b*) is written at each order by using the expressions (3.11) and (3.14) of the separation constants $G_0$ and $G_1$, and asymptotic solutions for $\lambda \to \infty$ are sought. The technical details of the calculation can be found in Appendix D (see also Fyrillas & Szeri 1994, 1995). The resulting asymptotic zeroth-order smooth field reads

$$C_{0,\infty}^{sm}(\sigma) = \exp\left[\beta\int_\sigma^\infty \frac{\langle B(\sigma',\tau)\rangle_\tau}{\langle A(\sigma',\tau)\rangle_\tau}\,\mathrm{d}\sigma'\right] - 1, \tag{4.4}$$

while the asymptotic first-order smooth field $C_{1,\infty}^{sm}$ is zero, so that (4.4) represents, in fact, the asymptotic smooth solution up to order $1/Pe$.

## 5. Numerical results

### 5.1. *Bubble dynamics*

We will consider hereafter the case of an argon bubble in a mixture of water and some other species at ambient temperature $T = 298$ K. The temporal evolution of the bubble radius is calculated by solving the Keller-Miksis equation (Keller & Miksis 1980; Hilgenfeldt, Lohse & Brenner 1996):

$$\begin{aligned}\tilde{R}\frac{\mathrm{d}^2\tilde{R}}{\mathrm{d}t^2}\left(1-\frac{1}{c}\frac{\mathrm{d}\tilde{R}}{\mathrm{d}t}\right) + \frac{3}{2}\left(\frac{\mathrm{d}\tilde{R}}{\mathrm{d}t}\right)^2\left(1-\frac{1}{3c}\frac{\mathrm{d}\tilde{R}}{\mathrm{d}t}\right)\\ = \frac{1}{\rho}\left\{\left(1+\frac{1}{c}\frac{\mathrm{d}\tilde{R}}{\mathrm{d}t}\right)[\tilde{p}_g - p_0(1-P\cos\omega t)] + \frac{\tilde{R}}{c}\frac{\mathrm{d}\tilde{p}_g}{\mathrm{d}t} - \frac{2\sigma}{\tilde{R}} - \frac{4\mu}{\tilde{R}}\frac{\mathrm{d}\tilde{R}}{\mathrm{d}t}\right\},\end{aligned} \tag{5.1}$$

where $\tilde{R}$ is the bubble radius, $\tilde{p}_g$ the gas pressure in the bubble, assumed homogeneous, $c = 1500\ \mathrm{m\,s^{-1}}$, $\rho = 998\ \mathrm{kg\,m^{-3}}$, $\mu = 10^{-3}\ \mathrm{kg\,m^{-1}\,s^{-1}}$ are, respectively,

the sound velocity, density and dynamic viscosity of water, $p_0 = 101325$ Pa the pressure in the liquid at rest, $\sigma = 0.072\ \mathrm{N\,m^{-1}}$ the water–gas surface tension, $P$ the dimensionless driving pressure amplitude and $\omega$ the angular driving frequency.

Two different models can be used for the bubble interior. The first assumes an isothermal behaviour and a van der Waals equation of state, so that the bubble internal pressure is

$$\tilde{p}_g = \left(p_0 + \frac{2\sigma}{\tilde{R}_0}\right)\left(\frac{\tilde{R}_0^3 - h^3}{\tilde{R}^3 - h^3}\right), \tag{5.2}$$

where $\tilde{R}_0$ is the ambient radius of the bubble and $h$ the van der Waals hard-core radius. A refined model accounting for water evaporation at the bubble wall and temperature gradients in the bubble was also used. The details of the model can be found in Toegel *et al.* (2000) and Storey & Szeri (2001). It is known that accounting for such effects reduces the violence of the collapse and may therefore influence the segregation process investigated in this paper, as will be seen below.

In the following sections, equation (5.1) will be solved for various sets of parameters $\omega$, $P$ and $\tilde{R}_0$, over a number of periods sufficiently large to obtain steady-state oscillations. The corresponding bubble volume and its time derivatives on the last period are stored in tables, from which the time- and space-dependent coefficients $A(\sigma, \tau)$ and $B(\sigma, \tau)$ can be calculated by equations (2.21 *a,b*) when required.

### 5.2. *Comparison with full simulation*

In order to check the validity of the approximation obtained from the splitting method, numerical simulations of the full convection–diffusion problem, (2.20)–(2.22), have been performed, with the help of the FEMLAB software. The present set of equations is recast without further difficulty in the canonical coefficient form of partial differential equations allowed in FEMLAB. The interval $[0, \infty]$ was mapped to $[0, 1]$ by using the variable change $x = 1/(\sigma + 1)$, the interval $[0, 1]$ was non-uniformly meshed to trap the boundary layer near the bubble wall, and mesh convergence studies were performed to ensure good accuracy of the result.

In order to test the analytical approximation obtained in the preceding section, we first recall that the analytical method yields the concentration field as

$$C(\sigma, \tau) = C_0^{sm}(\sigma, \lambda) + \frac{1}{Pe^{1/2}} C_1^{sm}(\sigma, \lambda) + \frac{1}{Pe^{1/2}} C_1^{osc}(\sigma, \tau) + O\left(\frac{1}{Pe}\right),$$

since $C_0^{osc} = 0$. For large times ($\lambda \to \infty$), $C_0^{sm}$ reaches its asymptotic limit $C_{0,\infty}^{sm}$ and as shown above, $C_1^{sm}$ vanishes. The oscillatory field $C_1^{osc}$ should reach its asymptotic value (3.13) in a few periods, and therefore one should have

$$C(\sigma, \tau) \underset{\lambda \to \infty}{\sim} C_{0,\infty}^{sm}(\sigma) + \frac{1}{Pe^{1/2}} \bar{C}_1^{osc}(\sigma, \tau) + O\left(\frac{1}{Pe}\right). \tag{5.3}$$

Further averaging on time $\hat{\tau}$ over one period, we obtain

$$\langle C(\sigma, \tau) \rangle_{\hat{\tau}} \underset{\lambda \to \infty}{\sim} C_{0,\infty}^{sm}(\sigma) + O\left(\frac{1}{Pe}\right), \tag{5.4}$$

since from equation (3.13), $\bar{C}_1^{osc}$ has a null $\hat{\tau}$-average.

Both equations (5.3) and (5.4) were checked against direct numerical simulation for an argon bubble of ambient radius $R_0 = 4\ \mu$m driven by pressure fields of dimensionless amplitudes $P = 0.3$, 0.6 and 0.8 and frequency 26.5 kHz. Since our aim is to check the analytical model against a numerical result, we take an arbitrary value $\beta = -10^{-5}$ rather than specifying species A mixed with water. In order to reach

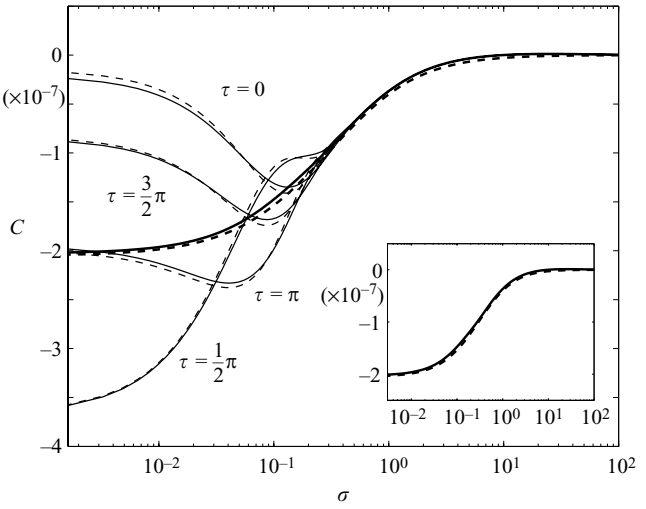


FIGURE 1. Comparison between the full numerical solution and the analytical approximation for a 4 μm argon bubble in water in a 26.5 kHz acoustic field of amplitude $P = 0.6$. The Péclet number is 500 and the parameter $\beta$ is $-10^{-5}$. Thin solid lines, concentration profiles $C^{num}(\sigma, \tau)$ obtained by numerical simulation at different phases of the bubble oscillation; thin dashed line, analytical predictions $C^{sm}_{0,\infty}(\sigma) + Pe^{-1/2}\bar{C}^{osc}_1(\sigma, \tau)$; thick solid line, nonlinear numerical average of the numerical profile over one period; thick dashed line, asymptotic zeroth-order smooth concentration profile $C^{sm}_{0,\infty}(\sigma)$. The inset shows a more detailed comparison between the numerical average and the smooth solution.

the limit $\lambda \to \infty$ numerically, the final time of the simulation was chosen sufficiently large that the system nearly reaches its steady state. The analysis of the smooth problem shows that its steady state should be obtained within a number of periods of the order of $Pe$. We therefore chose arbitrarily $Pe = 100$ and $Pe = 500$ in order to obtain reasonable simulation times. We found in our examples that no noticeable change from one period to the next could be observed after about $2Pe$ periods. The last oscillation period of the concentration field $C^{num}(\sigma, \tau)$ obtained numerically was stored, the nonlinear time $\hat{\tau}$ was calculated, and the nonlinear-average $\langle C^{num}(\sigma, \tau)\rangle_{\hat{\tau}}$ was calculated over one period at each spatial point $\sigma$. The smooth concentration field $C^{sm}_{0,\infty}(\sigma)$ was evaluated by calculating the integral in equation (4.4) with a Gauss–Jacobi method (see Louisnard & Gomez 2003, Appendix B for details). The asymptotic oscillatory field was calculated from equation (3.13), after evaluating the Fourier coefficients $h_m$ of $H(\hat{\tau})$ by a fast Fourier transform (FFT).

Figure 1 shows typical concentration profile results for a 4 μm argon bubble in water, driven by an oscillatory pressure of 0.6 bar amplitude and 26.5 kHz frequency, and $Pe = 500$. The dashed lines represent the analytical predictions and the solid ones are the numerical results. The total concentration profile (thin lines) is drawn at four distinct phases of the acoustic period in order to check equation (5.3). It is seen that the analytical predictions are in excellent agreement with the numerical result. We also display in figure 1 the average $\langle C^{num}(\sigma, \tau)\rangle_{\hat{\tau}}$ (thick solid line) along with the analytical prediction $C^{sm}_{0,\infty}(\sigma)$ (thick dashed line). It can be seen that both quantities are in excellent agreement (see the magnification in the inset) and we conclude that equation (5.4) is fulfilled. Besides, it is expected that the analytical approximation would progressively break as the asymptotic parameter $Pe^{-1/2}$ increases. Calculations with a smaller Péclet number ($Pe = 100$, not presented here), show that this is indeed the case, and yielded a maximum relative error on the oscillatory field amounting to 11%.

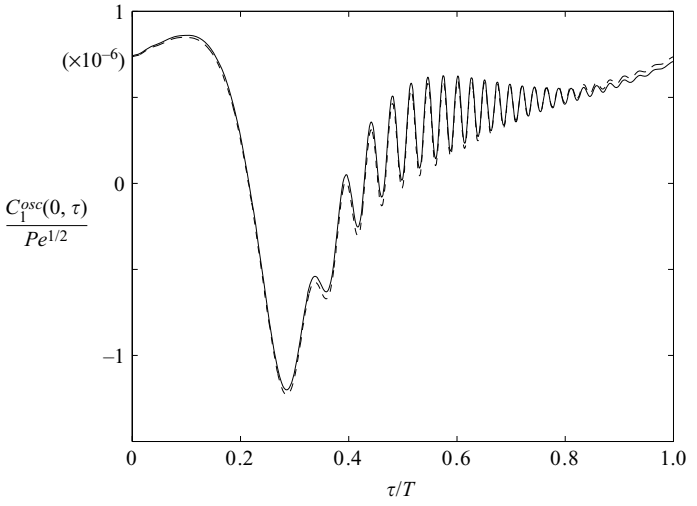


FIGURE 2. Comparison between the analytical oscillatory concentration (dashed line) $Pe^{-1/2}\bar{C}_1^{osc}(0,\tau)$ at the bubble wall and the numerical solution $C^{num}(0,\tau)-C_{0,\infty}^{sm}(0)$ (solid line) for a 4 μm argon bubble driven at $P=0.8$ and 26.5 kHz. The Péclet number is 100 and the parameter $\beta$ is $-10^{-5}$.

Another validation of the model can be seen in figure 2, which compares the oscillatory part of the numerical solution at the bubble wall $C^{num}(0,\tau)-C_{0,\infty}^{sm}(0)$ to the analytical solution $Pe^{-1/2}\bar{C}_1^{osc}(0,\tau)$ over one period of oscillation, for a driving pressure of amplitude $P=0.8$, and $Pe=100$: here again, the two results are in excellent agreement.

### 5.3. *Parameter-space exploration*

The validation of the analytical model being achieved, we now turn to investigate how the smooth and oscillatory parts vary with the bubble parameters ($R_0$, $P$, $\omega$). In order to obtain an immediate view of the magnitude of the segregation process, we will focus on the values of the two fields at the bubble wall.

#### 5.3.1. *Smooth part*

The smooth concentration at the bubble wall $C_{0,\infty}^{sm}(0)$ is obtained by setting $\sigma=0$ in equation (4.4):

$$C_{0,\infty}^{sm}(0)=\exp(\beta I)-1, \tag{5.5}$$

where

$$I=\int_0^{\infty}\frac{\langle B(\sigma',\tau)\rangle_\tau}{\langle A(\sigma',\tau)\rangle_\tau}\,\mathrm{d}\sigma'. \tag{5.6}$$

The value of integral $I$ depends only on the bubble dynamics, and in order to find a picture independent of the choice of a specific mixture, but containing all the bubble data, we use the definition (2.17) of the parameter $\beta$ to obtain

$$C_{0,\infty}^{sm}(0)=\exp(\beta_m\tilde{R}_0^2\omega^2 I)-1,$$

where $\beta_m$, defined by equation (2.18) depends only on the mixture considered. Thus, the value of $\tilde{R}_0^2\omega^2 I$ will be calculated for various bubble parameters and $C_{0,\infty}^{sm}(0)$ can then easily be deduced for a specific mixture.

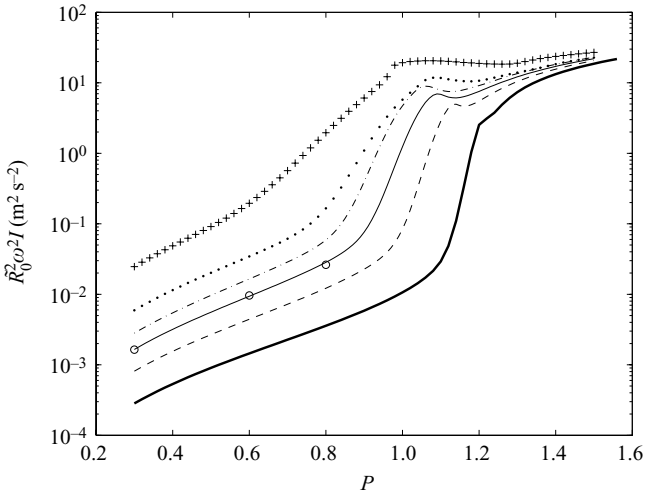


FIGURE 3. Evolution of $\tilde{R}_0^2\omega^2 I$ with driving pressure, from equation (5.6). The four bottom curves are calculated with $f = 26.5$ kHz, for ambient radii $\tilde{R}_0 = 2$ μm (thick solid line), 3 μm (dashed line), 4 μm (thin solid line), 5 μm (dash-dotted line). The two top curves are calculated for $\tilde{R}_0 = 4$ μm and, respectively, with $f = 50$ kHz (dotted line) and $f = 100$ kHz (+ signs). The three circles represents the results obtained by FEMLAB full simulations for 4 μm bubbles driven, respectively, by pressure fields of 0.3, 0.6 and 0.8 driving pressure.

Figure 3 represents $\tilde{R}_0^2\omega^2 I$ as a function of the driving pressure, for different ambient radii and different frequencies. The four bottom curves are calculated for a frequency of 26.5 kHz, for bubble ambient radii ranging from 2 μm to 5 μm. It can be seen that $\tilde{R}_0^2\omega^2 I$ increases with $\tilde{R}_0$ in the range considered. The three circles represent the value obtained from FEMLAB direct simulations, showing again the good agreement with analytical results. The two top curves are calculated for a 4 μm bubble excited, respectively, at 50 kHz (dotted line) and 100 kHz (+ signs): it can be seen that the mean segregation process increases markedly with frequency for small driving pressures, but that all curves merge for high driving pressures.

In all cases, a marked increase of $\tilde{R}_0^2\omega^2 I$ occurs near $P = 1$ which is approximately the Blake threshold (Akhatov *et al.* 1997; Hilgenfeldt *et al.* 1998; Louisnard & Gomez 2003). Above this driving pressure value, the bubble dynamics becomes inertially driven, yielding large time variations of $V(t)$ and its time derivatives, and therefore large values of the integrand in equation (5.6).

### 5.4. *Parameter-space exploration: oscillatory part*

Neglecting terms of order $O(Pe^{-1})$, the oscillatory concentration at the bubble wall $C^{osc}(0, \hat{\tau})$ reduces to $\bar{C}_1^{osc}(0, \hat{\tau})/Pe^{1/2}$. Evaluating equation (3.13) at $s = 0$, we obtain

$$C^{osc}(0, \hat{\tau}) = \frac{\beta}{Pe^{1/2}} \left[C_0^{sm}(0) + 1\right] G(\hat{\tau}), \tag{5.7}$$

where

$$G(\hat{\tau}) = \left(\frac{\hat{T}}{2\pi}\right)^{1/2} \sum_{\substack{m=-\infty \\ m\neq 0}}^{m=+\infty} \frac{h_m}{|m|^{1/2}} \exp\left[\mathrm{i}\left(2\pi m \frac{\hat{\tau}}{\hat{T}} - \epsilon_m \frac{\pi}{4}\right)\right]. \tag{5.8}$$

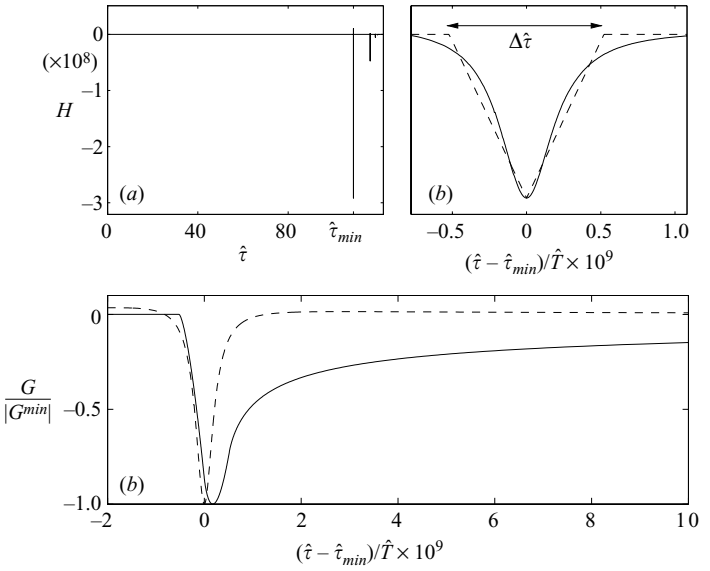


FIGURE 4. (*a*) Time evolution of function $H(\hat{\tau})$ for a 4 μm bubble driven at $P = 1.1$ and 26.5 kHz. The nonlinear period is 122 in this case. The negative peaks corresponds to the huge positive values taken by $\dot{V}$ at the main collapse and subsequent afterbounces. (*b*) Zoom on the most negative peak of $H(\hat{\tau})$ (solid line) translating the origin of abscissas to the location of this peak. The width of the peak is 9 orders of magnitude smaller than the nonlinear period; the dashed line is the approximation of $H(\hat{\tau})$ defined by (5.10). (*c*) Solid line, shape of function $G(\hat{\tau})$ given by equation (5.8); dashed line, shape of function $H(\hat{\tau})$.

Using equation (2.17) to express the factor $\beta/Pe^{1/2}$ in terms of the dimensional parameters, equation (5.7) becomes

$$\bar{C}_1^{osc}(0, \hat{\tau}) = \beta_m D^{1/2} \tilde{R}_0 \omega^{3/2} \left[C_0^{sm}(0) + 1\right] G(\hat{\tau}). \tag{5.9}$$

In order to identify the contribution of the bubble oscillations independently from the choice of a specific mixture, the quantity $\tilde{R}_0 \omega^{3/2} G(\hat{\tau})$ must be calculated for various bubble parameters. For small driving pressure, $G(\hat{\tau})$ can be evaluated by summing the series (5.8) without any specific problem, as was done in §5.2. However, for driving pressures high enough to yield inertial cavitation, evaluation of $G(\hat{\tau})$ is subject to a technical difficulty linked to the shape of function $H(\hat{\tau}) = -2\ddot{R}/R^2$ (figure 4*a*). Owing to the huge outward acceleration of the liquid at the end of the bubble collapse, $H(\hat{\tau})$ looks like a series of negative Dirac distributions, the most important being located at the main collapse, and the other ones at each secondary collapse between the bubble afterbounces. From the singular shape of function $H(\hat{\tau})$, it is expected that its Fourier spectrum (the coefficients $h_m$ in the series (3.12)) spans over a wide frequency range. Therefore, series (5.8) converges very slowly, thus forbidding any numerical estimation. This is illustrated in figure 4(*b*), which shows a magnification of the most negative peak of $H(\hat{\tau})$. It can be seen that the width of the peak is less than 9 orders of magnitude of the nonlinear period of oscillation, so that one should sum more than $10^9$ terms in the series to obtain an acceptable result.

We therefore used the following trick: let us denote $\hat{\tau}_{min}$ the time at which $H(\hat{\tau})$ reaches its highest negative peak amplitude $H_{min}$. We fit $H$ by a negative tooth

function of amplitude $H_{min}$ and width $\Delta\hat{\tau}$:

$$H(\hat{\tau}) \simeq \begin{cases} H_{min}\left(1 - \left|\dfrac{\hat{\tau} - \hat{\tau}_{min}}{\Delta\hat{\tau}}\right|\right), & \hat{\tau} \in [\hat{\tau}_{min} - \Delta\hat{\tau}, \hat{\tau}_{min} + \Delta\hat{\tau}], \\ 0, & \text{elsewhere}, \end{cases} \tag{5.10}$$

where $\Delta\hat{\tau}$ is determined in such a way that the real and fitted peaks have the same integral over the interval $[\hat{\tau}_1, \hat{\tau}_2]$, where $\hat{\tau}_1$ and $\hat{\tau}_2$ are the locations of the zeros of $H(\hat{\tau})$ at each side of $\hat{\tau}_{min}$:

$$\Delta\hat{\tau} = \frac{1}{H_{min}} \int_{\hat{\tau}_1}^{\hat{\tau}_2} H(\hat{\tau})\, \mathrm{d}\hat{\tau}. \tag{5.11}$$

$\Delta\hat{\tau}$ represents physically the characteristic time (in nonlinear form) of the bubble rebound at the end of the collapse. Figure 4(*b*) shows the original function $H(\hat{\tau})$ (solid line) compared to the approximation obtained by equation (5.10) (dotted line).

The Fourier coefficients of the tooth function can easily be calculated and introduced into equation (5.8) to calculate $G(\hat{\tau})$. This is done in Appendix E and the following approximation of $G(\hat{\tau})$ is obtained:

$$G_{app}(\hat{\tau}) = \left(\frac{\hat{T}}{2\pi}\right)^{1/2} H_{min} \frac{\hat{T}}{\pi^2 \Delta\hat{\tau}} \sum_{m=1}^{m=+\infty} \frac{1}{m^{5/2}} \sin^2\left(m\pi \frac{\Delta\hat{\tau}}{\hat{T}}\right) \cos\left[2m\pi \frac{\hat{\tau} - \hat{\tau}_{min}}{\hat{T}} - \frac{\pi}{4}\right]. \tag{5.12}$$

For very small $\Delta\hat{\tau}$, which is the case for inertial cavitation, this series is as difficult to calculate as the original one in (5.8). However, a good approximation of $G_{app}(\hat{\tau})$ can be found and is detailed in Appendix E (see equations (E 3) and (E 12)). Figure 4(*c*) shows the typical shape of $G_{app}(\hat{\tau})$: it decreases rapidly down to a minimum located slightly after the minimum of $H$ and then slowly relaxes to 0. We first restrain our primary interest to the extremal value attained by $\bar{C}_1^{osc}(0, \hat{\tau})$ over one period, so that only the minimum value of $G_{app}(\hat{\tau})$ is required. It is shown in Appendix E that an excellent estimate of this minimum is

$$G_{app}^{min} = \frac{8\Gamma(1/2)}{3\sqrt{3}\pi} H_{min} \Delta\hat{\tau}^{1/2}. \tag{5.13}$$

The solid line in figure 5 displays the evolution of $\tilde{R}_0\omega^{3/2}|G^{min}|$ obtained by summing directly series (5.8) along with a $2^{15}$ points FFT of $H(\hat{\tau})$, while the dashed line represents $\tilde{R}_0\omega^{3/2}|G_{app}^{min}|$ calculated from the approximate equation (5.13) for a 4 μm argon bubble oscillating at 26.5 kHz in water. Both results are in agreement up to about $P = 1.05$ ( which corresponds approximately to the Blake threshold) and they markedly diverge above the threshold, which demonstrates that for inertial motion of the bubble, $H(\hat{\tau})$ becomes too sharp to be represented correctly by a reasonable Fourier expansion. Therefore, in the inertial regime, the approximate equation (5.13) must be used to calculate $G^{min}$.

The dash-dotted line in figure 5 also displays the value of $\tilde{R}_0\omega^{3/2}|G_{app}^{min}|$ calculated from (5.13), but with a refined bubble interior model, taking into account heat transport and water condensation/evaporation at the bubble wall (Toegel *et al.* 2000; Storey & Szeri 2001). At low driving pressures, the results are comparable, but above the Blake threshold, the refined model predicts values lower by one order of magnitude. Such a result could be expected since it is known that taking into account heat transport in the bubble interior yields a less violent collapse than with the isothermal model, and therefore decreases the amplitude of function $H$. Similar conclusions have been drawn for other bubble phenomena directly linked to the

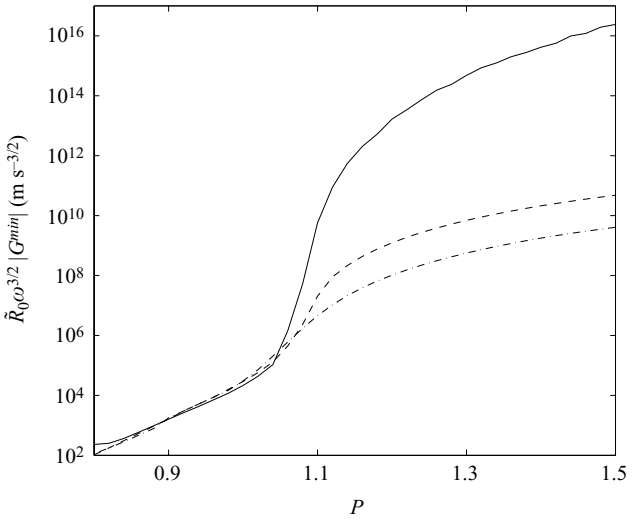


FIGURE 5. Solid line, evolution of $\tilde{R}_0\omega^{3/2}|G^{min}|$ calculated by summing the series in (5.8) from a $2^{15}$ points FFT of $H(\hat{\tau})$; dashed line, $\tilde{R}_0\omega^{3/2}|G^{min}_{app}|$ calculated from (5.13). Both curves are obtained for a 4 μm argon bubble excited at 26.5 kHz, assuming an isothermal gas behaviour. The dash-dotted line also represents the evolution of $\tilde{R}_0\omega^{3/2}|G^{min}_{app}|$, but calculated with the refined model of the bubble interior. The values obtained are about one order of magnitude smaller than with the isothermal model.

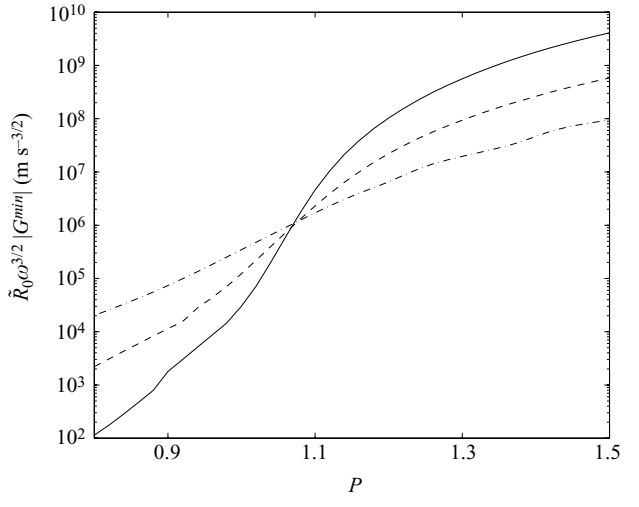


FIGURE 6. Evolution of $\tilde{R}_0\omega^{3/2}|G^{min}_{app}|$ calculated from (5.13), for a 4 μm argon-bubble excited at 26.5 kHz (solid line), 50 kHz (dashed line) and 100 kHz (dash-dotted line). The bubble interior refined model was used in all cases.

violence of the collapse, such as Rayleigh–Taylor shape instabilities (Lin, Storey & Szeri 2002). Since the refined model is believed to be more realistic than the isothermal one, it will be used in every result presented hereinafter.

Figure 6 displays the influence of frequency on the oscillatory field. As frequency increases, there is a stronger effect at low amplitude but, for high amplitudes, increasing the frequency reduces the oscillatory segregation effect, despite the $\omega^{3/2}$ scaling law. This can be explained easily by the fact that increasing the frequency limits the

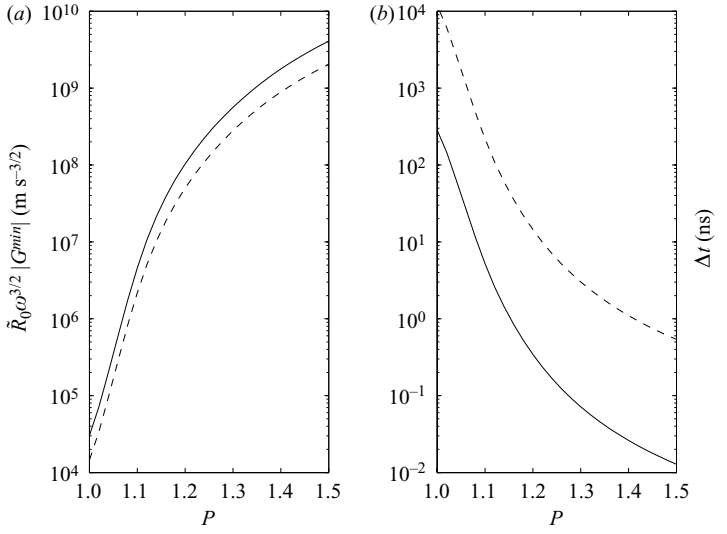


FIGURE 7. (*a*) Comparison of $\tilde{R}_0\omega^{3/2}|G^{min}_{app}|$ evaluated from (5.13) (solid line) and from (5.15) (dashed line) for a 4 μm argon bubble excited at 26.5 kHz. (*b*) Characteristic time $\Delta t$ of the bubble rebound for the same bubble, calculated from (5.16) (solid line). The dashed line represents $42\Delta t$, which is the time necessary for the oscillatory segregation to reach one tenth of its maximum value.

expansion phase of the bubble in the inertial regime, which in turn reduces the violence of the collapse, and therefore the peak value attained by the $H$ function.

Finally, a more practical sense can be given to the time-interval $\Delta\hat{\tau}$ appearing in (5.13): since $H(\hat{\tau}) = -2\ddot{R}/R^2$, and using the definition (3.1) of the nonlinear time, (5.11) can also be expressed as

$$\Delta\hat{\tau} = \frac{-2}{H_{min}} \int_{\tau_1}^{\tau_2} R^2(\tau)\ddot{R}(\tau)\,\mathrm{d}\tau.$$

Times $\tau_1$ and $\tau_2$ are located, respectively, closely before and closely after the time at which the bubble reaches its minimum radius. Therefore, $R$ stays close to $R_{min}$ in the interval $[\tau_1, \tau_2]$, so that $H_{min} \simeq -2\ddot{R}_{max}/R^2_{min}$. Therefore,

$$\Delta\hat{\tau} \simeq \frac{R^4_{min}(\dot{R}(\tau_2) - \dot{R}(\tau_1))}{\ddot{R}_{max}},$$

and since by definition $\tau_1$ and $\tau_2$ are the zeros of $\ddot{R}$, $\dot{R}(\tau_1)$ and $\dot{R}(\tau_2)$ are the minimum and maximum bubble velocities attained before and after the rebound, respectively, which are in fact the minimum and maximum velocities of the bubble over one acoustic period. Thus,

$$\Delta\hat{\tau} \simeq R^4_{min}\frac{\dot{R}_{max} - \dot{R}_{min}}{\ddot{R}_{max}}. \tag{5.14}$$

Injecting this value into (5.13), and setting $H_{min} \simeq -2\ddot{R}_{max}/R^2_{min}$, we obtain

$$G^{min}_{app} \simeq -\frac{8\Gamma(1/2)}{3\sqrt{3}\pi}[\ddot{R}_{max}(\dot{R}_{max} - \dot{R}_{min})]^{1/2}, \tag{5.15}$$

which can easily be evaluated once the bubble dynamics is known. Figure 7(*a*) shows that equation (5.15) gives a reasonable approximation of $G^{min}_{app}$.

Apart from the minimum value reached by $G$, it is also of interest to obtain an order of magnitude of the relaxation time of $G$ (see solid line figure 4$c$). It is shown in Appendix E that $G$ reaches one tenth of its minimum value after a relaxation time of $42\Delta\hat{\tau}$ past $\hat{\tau}_{min}$. Evaluating $\Delta\hat{\tau}$ from (5.14), a ready-to-use estimate of the oscillatory segregation duration can be obtained. The dimensional rebound time $\Delta t$ corresponding to $\Delta\hat{\tau}$ can be obtained by first converting the latter in linear time by $\Delta\tau \simeq \Delta\hat{\tau}/R_{min}^4$ and setting $\Delta t = \Delta\tau/\omega$. We obtain:

$$\Delta t \simeq \frac{1}{\omega}\frac{\dot{R}_{max} - \dot{R}_{min}}{\ddot{R}_{max}}. \tag{5.16}$$

Figure 7($b$) displays the dimensional rebound characteristic time $\Delta t$ in ns (solid line) for a 4 μm argon bubble at 26.5 kHz: it rapidly drops from about 300 ns for $P = 1$ to 10 ps for $P = 1.5$. For practical applications, the dashed line represents $42\Delta t$, during which the oscillatory segregation stays larger than one tenth of its maximal value. This is a valuable result, if one wishes to compare the segregation duration to a characteristic time of some process likely to be enhanced by species segregation.

## 6. Application and discussion

The above results should now be applied to real binary mixtures to assess the importance of the phenomenon. Rather than selecting specific mixtures, we will try to cover a wide range of molecule sizes by taking typical values for the other mixture parameters.

We first combine equations (2.14), (5.5) and (5.7) to obtain the segregation ratio at the bubble wall

$$\frac{\omega_A(0,\hat{\tau})}{\omega_{A0}} = \exp(\beta I)\left(1 + \frac{\beta}{Pe^{1/2}}G(\hat{\tau})\right). \tag{6.1}$$

Having practical applications in view, we are interested in the average and peak concentrations at the bubble wall, so that in what follows, we will calculate the two quantities:

$$\Omega_m = \exp(\beta I), \tag{6.2a}$$

$$\Delta\Omega_m = \exp(\beta I)\frac{\beta}{Pe^{1/2}}G^{min}, \tag{6.2b}$$

where $G^{min} < 0$ is calculated from (5.13). The two quantities $\Omega_m$ and $\Delta\Omega_m$ should be interpreted as follows: the first is the average concentration at the bubble wall and the second is the maximum algebraic variation of the concentration around the average, over an oscillation period.

Before specifying the mixture, it is worth recalling that $\beta$ depends on two physical properties (see (2.18)): on one hand, the relative densities of species A and the host liquid, on the other hand, the molar weight of species A. The latter may vary in a much larger range than the former, so that in what follows, we will study the predictions of the model for a mixture of water with a heavier species A of apparent density $\rho_A = M_A/\bar{V}_A = 2000\ \mathrm{kg\,m^{-3}}$, and molecular weights $M_A$ ranging from 100 to $10^7$ Da (1 Dalton corresponds to a molar weight of 1 $\mathrm{g\,mol^{-1}}$).

The temperature of the mixture is set to $T = 298\ \mathrm{K}$. Consistently with the dilute mixture hypothesis detailed in Appendix A, the density $\rho$ of the mixture is approximated by the density of pure water. To calculate the oscillatory part under the same conditions, the additional datum of the diffusion coefficient is required. Since we consider a set of species where molecular weight varies over a wide range, the influence

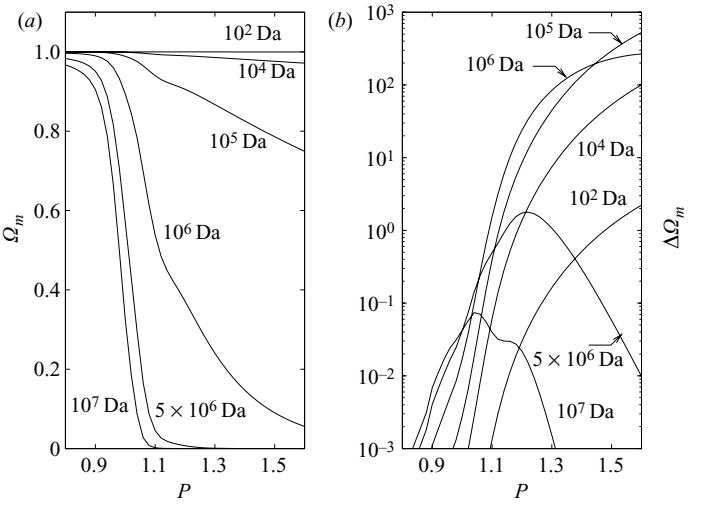


FIGURE 8. Segregation ratio in a mixture of water with molecules of apparent density 2000 kg m$^{-3}$, of molecular weight $M_A$ ranging from 100 to $10^7$ Da around a 4 μm argon bubble driven at 26.5 kHz: (*a*) smooth segregation ratio defined by (6.2*a*), (*b*) oscillatory peak segregation ratio defined by (6.2*b*).

of the molecular size on the diffusion coefficient $D$ should be taken into account. Following the Stokes–Einstein theory, the diffusion coefficient can be expressed as

$$D = \frac{k_B T}{6\pi\mu R_A}, \tag{6.3}$$

where $k_B$ is the Boltzmann constant and $R_A$ the hydrodynamic radius, estimated from the molecular weight and apparent density of species A by

$$\mathcal{N}_a \tfrac{4}{3}\pi R_A^3 \rho_A = M_A, \tag{6.4}$$

where $\mathcal{N}_a$ is the Avogadro number. Under these conditions, the parameter $\tilde{\beta}_m$ defined by (2.18) ranges from $-10^{-5}$ to $-1$ s$^2$ m$^{-2}$, the hydrodynamic radius from 0.27 to 12.5 nm, and the diffusion coefficient from $7.9 \times 10^{-10}$ to $1.7 \times 10^{-11}$ m$^2$ s$^{-1}$.

We consider the case of a 4 μm argon bubble excited at $f = 26.5$ kHz. The corresponding Péclet number for the above conditions ranges from 3 360 to 15 600, which justifies *a posteriori* the asymptotic expansions in terms of $Pe^{-1/2}$, and the non-dimensional parameter $\beta$ ranges from $-4.6 \times 10^{-6}$ to $-4.6 \times 10^{-1}$.

The order of magnitude of the average bubble wall concentration of such molecules is shown in figure 8(*a*): the $\Omega_m$ curve for the smallest molecules ($M_A = 100$ Da) remains indistinguishable from 1, even for high driving pressure, so that the mixture is unsegregated on average. As the weight of the molecules increases, their average depletion at the bubble wall becomes increasingly high for a given driving pressure. A nearly total depletion of the heaviest molecules ($M_A = 5 \times 10^6$ and $10^7$ Da) can even be observed for driving pressures slightly above the Blake threshold.

The amplitude of the oscillatory concentration variation $\Delta\Omega_m$ is shown in figure 8(*b*), where it can be seen that the smallest molecule is already over-concentrated by a factor of 2 at $P = 1.5$. As $M_A$ increases, $\Delta\Omega_m$ first increases, and then decreases again for very large molecules. This illustrates the opposite effects of the two factors $\exp(\beta I)$ and $\beta Pe^{-1/2} G^{min}$ in (6.2*b*). For the smallest molecules, the increase of $|G^{min}|$

with $P$ dominates over the decrease of $\exp(\beta I)$, so that $\Delta\Omega_m$ globally increases with driving pressure, up to nearly 500 for $M_A = 100\,000$ Da and $P = 1.6$. For larger molecules, the opposite occurs, so that the peak value $\Delta\Omega_m$ becomes increasingly masked by the strong average depletion $\Omega_m$ and hardly departs from 0 for $M_A = 10^7$ Da.

Thus, it is seen that both average depletion and peak periodic over-concentration at the bubble wall compete, depending on the driving level and the molecule sizes. This suggests that molecules or nano-particles that could undergo some growth or agglomeration process would be periodically concentrated against the bubble wall as long as they are sufficiently small, but would be held far from the bubble on average, as they reach some critical size. This may have some strong consequences on polymerization or nano-particle agglomeration processes, for example.

The present results may also help us to understand the positive effect of acoustic cavitation on crystal nucleation from a solute (see for example Lyczko *et al.* 2002, for potassium sulfate crystallization). Homogeneous nucleation of crystals in liquids is a first-order phase transition, which occurs as the solute concentration exceeds the saturation concentration. There is a fairly general agreement on the so-called classical nucleation theory (Kaschiev 2000), which states that in a metastable solution, the nucleation process occurs through progressive accumulation of solute molecules, forming multi-mers called 'clusters', up to a critical radius called nucleus, from which a solid crystal is then free to grow. There is indeed experimental evidence of the existence of such clusters, and their stratification under gravity has been observed in a sedimentation column (Mullin & Leci 1969; Larson & Garside 1986). Although stated differently by these authors, the process invoked to explain cluster sedimentation obeys the pressure diffusion equation considered in this paper. We may therefore reasonably conjecture that the pressure diffusion effect around an oscillating bubble would also tend to segregate these clusters to a much larger extent than gravity, in view of the respective accelerations involved. The present conclusions show that this is indeed the case, and predict that if the nucleating species is heavier than the liquid, its clusters would be periodically pushed against the bubble wall. There, since the collision probability varies with the square of the concentration, they could undergo more frequent attachment events and create larger clusters. Above a critical size, these clusters would then be held far from the bubble in the liquid, as suggested by figure 8(*a*).

The conclusions on the smooth effect should be tempered by considerations on the bubble stability. The smooth effect requires a very large number of acoustic periods to build up, so that its potential appearance is conditioned by the bubble stability on such a large time scale. If this stability is well established in single-bubble experiments, there is no definitive conclusion in multi-bubble fields. This issue has been discussed by Louisnard & Gomez (2003). Even in the most optimistic case, inertial bubbles would rapidly increase their size by rectified diffusion up to the fragmentation threshold, in a time too small for the smooth effect to build up completely. However, partial build-up remains possible, and may yield a noticeable smooth effect on the largest molecules.

Finally, despite the compressibility effects being arbitrarily neglected to reduce the mathematical complexity of the problem, it is nevertheless an important issue. A spherical shock wave can build up when the bubble rebounds after the collapse, and the corresponding steepening of the pressure profile may therefore enhance the oscillatory effect. Such spherical shocks are non-monotonic (see for example figures 7 and 8 of Fujikawa & Akamatsu 1980) so that just after the collapse, the heaviest species would be concentrated in a thin layer of fluid surrounding the shock, and would travel with the shock. An important consequence of this feature is that the excess concentration would not remain located near the bubble wall, but would be

transported toward the bulk liquid. In summary, shock-waves would not only enhance the oscillatory effect, but they may also extend its influence to a larger spatial region.

## 7. Conclusion

We have proposed an analytic method to solve the general problem of pressure-gradient-forced diffusion of two non-volatile species around a bubble oscillating radially in the mixture. The method yields the concentration field in the mixture around the bubble in two parts: a smooth part, building over a number of acoustic periods of the order of the Péclet number *Pe* and asymptotically constant in time, and an oscillatory part. Both expressions are fully analytic and can be easily calculated for a given bubble dynamics.

In the case of inertial cavitation, the oscillatory effect results in a large excess concentration of the heaviest species at the bubble wall at each bubble collapse. This excess is noticeable even for small molecules, and relaxes with a characteristic time which is more than one order of magnitude larger than the characteristic duration of the bubble rebound. Conversely, the smooth effect pushes the heaviest species far from the bubble. It remains unimportant for small molecules, even for strong driving pressures, but may almost deplete the bubble wall of large molecules. Both smooth and oscillatory effects increase with driving pressure. The smooth effect increases with the frequency of the driving. The oscillatory effect increases with frequency for small driving pressure, but conversely, decreases with frequency in the inertial regime.

For large molecules or nano-particles around an inertial bubble, the two smooth and oscillatory effects compete: the oscillatory effect dominates for the smallest molecules, while the smooth one is prominent for the largest ones. This has strong implications for any physico-chemical process involving molecules or particles undergoing a growing or agglomeration process, and suggests that species smaller than a given size would be periodically pushed and concentrated near the bubble wall, while the largest ones are on average held far from the bubble. Polymerization, agglomeration or cluster formation in crystal nucleation fall in this specific case and this behaviour may be partly responsible for the reported enhancement of nucleation by cavitation.

This work is supported by an ECOS-South collaboration program between France and Chile under grant number C03E05.

## Appendix A. Linearization of the convection–diffusion equation

We assume an ideal mixture of two liquids, so that volume is additive. Under these conditions, the mean density of the mixture is

$$\rho = \frac{x_A M_A + x_B M_B}{x_A \bar{V}_A + x_B \bar{V}_B}, \tag{A 1}$$

where $x_i$, $M_i$ and $\bar{V}_i$ are the mole fraction, molecular weight and partial molal volume of species i, respectively. Using the relation $x_i = M\omega_i/M_i$ between mole and mass fraction, we readily obtain

$$\rho = \frac{1}{\omega_A \bar{v}_A + \omega_B \bar{v}_B}, \tag{A 2}$$

where the notation $\bar{v}_i = \bar{V}_i/M_i$ has been used. The mean molecular weight of the mixture is defined by

$$\frac{1}{M} = \frac{\omega_A}{M_A} + \frac{\omega_B}{M_B}. \tag{A 3}$$

Replacing $\omega_B$ by $1-\omega_A$, we can express the density of the solution by

$$\rho = \frac{1}{\bar{v}_B}\left[1+\alpha_1\omega_A\right]^{-1},$$

and the two contributions to diffusion in (2.6) become

$$\rho\nabla\omega_A = \frac{1}{\bar{v}_B}\left[1+\alpha_1\omega_A\right]^{-1}\nabla\omega_A, \tag{A 4a}$$

$$\frac{M_A M_B}{M\mathscr{R}T}\omega_A\left(\frac{\bar{V}_A}{M_A}-\frac{1}{\rho}\right)\nabla p = \frac{M_A}{\mathscr{R}T}\alpha_1\omega_A\frac{(1-\omega_A)(1+\alpha_2\omega_A)}{1+\alpha_1\omega_A}\nabla p, \tag{A 4b}$$

where parameters $\alpha_1$ and $\alpha_2$ are defined by:

$$\alpha_1 = \frac{\bar{v}_A}{\bar{v}_B}-1, \quad \alpha_2 = \frac{M_B}{M_A}-1. \tag{A 5a, b}$$

Therefore, it can be seen that if we neglect terms of order $O(\omega_A^2)$, $O(\alpha_1^2\omega_A^2)$ and $O(\alpha_2^2\omega_A^2)$, equation (2.6) becomes

$$\frac{1}{\bar{v}_B}\left(\frac{\partial\omega_A}{\partial t}+\boldsymbol{v}\cdot\nabla\omega_A\right) = D\frac{1}{\bar{v}_B}\nabla\cdot\left[\nabla\omega_A+\frac{M_A}{\mathscr{R}T}\omega_A(\bar{v}_A-\bar{v}_B)\nabla p\right], \tag{A 6}$$

which is equation (2.7).

## Appendix B. Solution of the oscillatory problem and splitting

Each member of the hierarchy of oscillatory problems may be expressed as a non-homogeneous diffusion partial differential equation

$$\frac{\partial C_i^{osc}}{\partial\hat{\tau}}-\frac{\partial^2 C_i^{osc}}{\partial s^2} = F^i\left(R(\hat{\tau}), s, C_0^{osc}, \ldots, C_{i-1}^{osc}\right), \tag{B 1}$$

with a Neumann inhomogeneous boundary condition of the form:

$$\frac{\partial C_i^{osc}}{\partial s}(s=0,\hat{\tau}) = B^i\left(R(\hat{\tau}), C_{i-1}^{osc}\right). \tag{B 2}$$

We treat the problem in the manner of Fyrillas & Szeri (1995), with the difference that here we have a Neumann condition rather than a Dirichlet one.

The oscillatory solution $C_i^{osc}$ should vanish for $s\to+\infty$ since the outer solution of the boundary-layer problem is imposed to be identically 0. The asymptotic oscillatory solutions $\bar{C}^{osc}$ at any order have $T$ periodicity in the $\tau$ variable, and therefore $\hat{T}=\hat{\tau}(T)$ periodicity in the $\hat{\tau}$ variable. Thus, the functions $F^i$ and $B^i$ are also periodic in $\hat{\tau}$ and we expand them in Fourier series, as well as $\bar{C}^{osc}$. Setting $\omega_m = 2m\pi/\hat{T}$, we obtain

$$\bar{C}_i^{osc}(s,\hat{\tau}) = \sum_{m=-\infty}^{m=+\infty} c_m(s)\exp(\mathrm{i}\omega_m\hat{\tau}),$$

$$F^i(s,\hat{\tau}) = \sum_{m=-\infty}^{m=+\infty} f_m(s)\exp(\mathrm{i}\omega_m\hat{\tau}),$$

$$B^i(\hat{\tau}) = \sum_{m=-\infty}^{m=+\infty} b_m\exp(\mathrm{i}\omega_m\hat{\tau}).$$

Substituting these series in the problem (B 1)–(B 2), we obtain a set of differential equations relating the coefficients of these series. For any $m \neq 0$, we obtain

$$\frac{\mathrm{d}^2 c_m(s)}{\mathrm{d}s^2} - \mathrm{i}\omega_m c_m(s) = -f_m(s), \tag{B 3}$$

$$\frac{\mathrm{d}c_m(s)}{\mathrm{d}s}(s=0) = b_m. \tag{B 4}$$

The general solution of (B 3) vanishing for $s \to \infty$ is

$$c_m(s) = A_m \exp(-k_m s) - \frac{1}{k_m}\int_s^\infty f_m(s')\sinh[k_m(s-s')]\,\mathrm{d}s', \tag{B 5}$$

with

$$k_m = (1+\epsilon_m \mathrm{i})\left(\frac{|\omega_m|}{2}\right)^{1/2} = \left(\frac{2|m|\pi}{\hat{T}}\right)^{1/2} e^{\mathrm{i}\epsilon_m \pi/4},$$

where $\epsilon_m = \mathrm{sgn}(m)$. The boundary condition at $s=0$, (B 4), yields the following expression for $A_m$:

$$A_m = -\frac{b_m}{k_m} - \frac{1}{k_m}\int_0^\infty f_m(s')\cosh(k_m s')\,\mathrm{d}s'. \tag{B 6}$$

The zeroth-order harmonics differential equation ($m=0$) takes a different form:

$$\frac{\mathrm{d}^2 c_0(s)}{\mathrm{d}s^2} = -f_0(s),$$

with the associated boundary condition

$$\frac{\mathrm{d}c_0(s)}{\mathrm{d}s}(s=0) = b_0.$$

The solution vanishing for $s=\infty$ is

$$c_0(s) = \int_\infty^s \int_{s'}^\infty f_0(s'')\,\mathrm{d}s''\,\mathrm{d}s'.$$

Applying the Neumann boundary condition at $s=0$ yields:

$$b_0 = \int_0^\infty f_0(s')\,\mathrm{d}s',$$

and recognizing that $b_0 = \langle B^i \rangle_{\hat{\tau}}$ and $f_0(s) = \langle F^i(s)\rangle_{\hat{\tau}}$, the separation condition finally reads

$$\langle B^i \rangle_{\hat{\tau}} = \int_0^{+\infty} \langle F^i(s)\rangle_{\hat{\tau}}\,\mathrm{d}s. \tag{B 7}$$

Finally, in the special case where $F^i$ is identically zero, which is the case in the present paper for $i=1$, the separation condition merely implies that $\langle B^i \rangle_{\hat{\tau}}$ should be 0, and the oscillatory field reads in this case:

$$\bar{C}_i^{osc}(0,\hat{\tau}) = -\left(\frac{\hat{T}}{2\pi}\right)^{1/2} \sum_{\substack{m=-\infty \\ m\neq 0}}^{m=+\infty} \frac{b_m}{|m|^{1/2}} \exp\left[\mathrm{i}\left(2\pi m\frac{\hat{\tau}}{\hat{T}} - \epsilon_m\frac{\pi}{4}\right) - (\epsilon_m \mathrm{i}+1)\left(\frac{|m|\pi}{\hat{T}}\right)^{1/2} s\right]. \tag{B 8}$$

The presence of both $m^{1/2}$ in the denominator and the $\pi/4$ phase lag recalls the fact that $\bar{C}_i^{osc}(0,\hat{\tau})$ is the half-order integral of $B^i(\hat{\tau})$ as could be proved directly by solving problem (B 1), (B 2) by Laplace transforms.

## Appendix C. Solution of the second-order oscillatory problem

The second-order oscillatory problem reads

$$\frac{\partial C_2^{osc}}{\partial \hat{\tau}} = \frac{\partial^2 C_2^{osc}}{\partial s^2} + \frac{\partial}{\partial s}\left[A_1' s \frac{\partial C_1^{osc}}{\partial s} + \beta B_0' C_1^{osc}\right], \tag{C 1a}$$

$$\frac{\partial C_2^{osc}}{\partial s}(0,\hat{\tau}) + \beta H(\hat{\tau}) C_1^{osc}(0,\hat{\tau}) = -G_1 - \beta H(\hat{\tau}) C_1^{sm}(0,\tau), \tag{C 1b}$$

$$C_2^{osc}(s \to \infty) = 0. \tag{C 1c}$$

The splitting condition (B 7) reads therefore:

$$\left\langle -\beta H(\hat{\tau}) C_1^{osc}(0,\hat{\tau}) - G_1 - \beta H(\hat{\tau}) C_1^{sm}(0,\tau)\right\rangle_{\hat{\tau}} = \left\langle \int_0^\infty \frac{\partial}{\partial s}\left(A_1' s \frac{\partial C_1^{osc}}{\partial s} + \beta B_0' C_1^{osc}\right) \mathrm{d}s \right\rangle_{\hat{\tau}}. \tag{C 2}$$

Using (3.8) and (3.10*c*), the integral on the right-hand side of (C 2) can also be written as

$$\lim_{s\to\infty}\left(A_1' s \frac{\partial C_1^{osc}}{\partial s}(s,\hat{\tau})\right) - \beta H(\hat{\tau}) C_1^{osc}(0,\hat{\tau}). \tag{C 3}$$

It can be seen from (3.13) that the first term of (C 3) is zero, so that (C 2) finally becomes

$$G_1 = -\beta\left\langle H(\hat{\tau})\left[C_1^{sm}(0,\tau)\right]\right\rangle_{\hat{\tau}}. \tag{C 4}$$

## Appendix D. Solution of the smooth problem

The second- and third-order smooth equations are

$$\frac{\partial C_2^{sm}}{\partial \tau} = -\frac{\partial C_0^{sm}}{\partial \lambda} + \frac{\partial}{\partial \sigma}\left[A(\sigma,\tau)\frac{\partial C_0^{sm}}{\partial \sigma} + \beta B(\sigma,\tau)\left(C_0^{sm}+1\right)\right], \tag{D 1a}$$

$$\frac{\partial C_3^{sm}}{\partial \tau} = -\frac{\partial C_1^{sm}}{\partial \lambda} + \frac{\partial}{\partial \sigma}\left[A(\sigma,\tau)\frac{\partial C_1^{sm}}{\partial \sigma} + \beta B(\sigma,\tau) C_1^{sm}\right]. \tag{D 1b}$$

The expansion (4.2) must be uniformly valid and therefore should not contain secular terms increasing unbounded when $\tau \to \infty$. This non-secular behaviour will be satisfied by $C_2^{sm}$ and $C_3^{sm}$ only if the right-hand sides of equations (D 1 *a*,*b*) have zero $\tau$-averages. Therefore, $C_0^{sm}$ and $C_1^{sm}$ should fulfil the respective non-secularity conditions

$$\frac{\partial C_0^{sm}}{\partial \lambda} = \frac{\partial}{\partial \sigma}\left[\langle A(\sigma,\tau)\rangle_\tau \frac{\partial C_0^{sm}}{\partial \sigma} + \beta\langle B(\sigma,\tau)\rangle_\tau\left(C_0^{sm}+1\right)\right], \tag{D 2a}$$

$$\frac{\partial C_1^{sm}}{\partial \lambda} = \frac{\partial}{\partial \sigma}\left[\langle A(\sigma,\tau)\rangle_\tau \frac{\partial C_1^{sm}}{\partial \sigma} + \beta\langle B(\sigma,\tau)\rangle_\tau C_1^{sm}\right], \tag{D 2b}$$

where the independence of $C_0^{sm}$ and $C_1^{sm}$ on $\tau$ has been used.

The associated boundary conditions at the bubble wall, (2.24*b*), can be obtained from the separation constants $G_0$ and $G_1$, (3.11) and (3.74). Further using the

independence of $C_0^{sm}$ and $C_1^{sm}$ on the fast variable $\tau$, these boundary conditions are

$$\frac{\partial C_0^{sm}}{\partial \sigma}(0,\lambda) + \beta \langle H(\hat{\tau})\rangle_{\hat{\tau}} \left[C_0^{sm}(0,\lambda)+1\right] = 0, \tag{D 3a}$$

$$\frac{\partial C_1^{sm}}{\partial \sigma}(0,\lambda) + \beta \langle H(\hat{\tau})\rangle_{\hat{\tau}} C_1^{sm}(0,\lambda) = 0. \tag{D 3b}$$

Moreover, from the definition (2.25) of $H$, the nonlinear average $\langle H(\hat{\tau})\rangle_{\hat{\tau}}$ is also

$$\langle H\rangle_{\hat{\tau}} = \left\langle \frac{B(0,\tau)}{A(0,\tau)} \right\rangle_{\hat{\tau}} = \frac{\left\langle V^{4/3} B(0,\tau)/A(0,\tau)\right\rangle_\tau}{\langle V^{4/3}\rangle_\tau} = \frac{\langle B(0,\tau)\rangle_\tau}{\langle A(0,\tau)\rangle_\tau},$$

since $A(0,\tau) = V^{4/3}$, so that the zeroth- and first-order boundary conditions, (D 3 *a,b*), at the bubble wall may also be written as

$$\langle A(0,\tau)\rangle_\tau \frac{\partial C_0^{sm}}{\partial \sigma}(0,\lambda) + \beta \langle B(0,\tau)\rangle_\tau \left[C_0^{sm}(0,\lambda)+1\right] = 0, \tag{D 4a}$$

$$\langle A(0,\tau)\rangle_\tau \frac{\partial C_1^{sm}}{\partial \sigma}(0,\lambda) + \beta \langle B(0,\tau)\rangle_\tau C_1^{sm}(0,\lambda) = 0. \tag{D 4b}$$

We now seek the asymptotic solutions $C_{i,\infty}^{sm}$ for $i = 0, 1$ of (D 2 *a,b*), by setting $\partial C_{i,\infty}^{sm}/\partial\lambda = 0$ for $i = 0, 1$ in these equations and integrating once with respect to $\sigma$. Making use of boundary conditions (D 4 *a,b*), this integration yields

$$\langle A(\sigma,\tau)\rangle_\tau \frac{\partial C_{0,\infty}^{sm}}{\partial \sigma} + \beta \langle B(\sigma,\tau)\rangle_\tau \left(C_{0,\infty}^{sm}+1\right) = 0, \tag{D 5a}$$

$$\langle A(\sigma,\tau)\rangle_\tau \frac{\partial C_{1,\infty}^{sm}}{\partial \sigma} + \beta \langle B(\sigma,\tau)\rangle_\tau C_{1,\infty}^{sm} = 0. \tag{D 5b}$$

Now using the condition at infinity, (2.26), the zeroth-order (D 5*a*) can be integrated as

$$C_{0,\infty}^{sm}(\sigma) = \exp\left[\beta \int_\sigma^\infty \frac{\langle B(\sigma',\tau)\rangle_\tau}{\langle A(\sigma',\tau)\rangle_\tau}\, \mathrm{d}\sigma'\right] - 1. \tag{D 6}$$

Besides, integration of the first-order equation (D 5*b*) can only yield the null solution $C_{1,\infty}^{sm} = 0$ in order to fulfil the condition at infinity, (2.26). It does not imply, however, that $C_1^{sm}(\sigma,\lambda)$ is zero for finite $\lambda$, but merely states that its asymptotic limit for $\lambda \to \infty$ is zero.

The physical meaning of the asymptotic smooth solution may be understood from (D 5 *a,b*). The average pressure diffusion flux (the $B$ term) is exactly balanced by the average Fick diffusion flux (the $A$ term), and therefore the smooth concentration field stays constant. The unsteady term in the smooth equations (D 2 *a,b*) represents the transitory non-equilibrium between the two average diffusion processes.

## Appendix E. Numerical estimation of the oscillatory asymptotic concentration field

We first set $x = 2\pi\hat{\tau}/\hat{T}$, $x_{min} = 2\pi\hat{\tau}_{min}/\hat{T}$ and $\Delta x = 2\pi\Delta\hat{\tau}/\hat{T}$ . In the new variable $x$, the tooth-approximation (5.10) can be written as

$$H(x) \simeq \begin{cases} H_{min}\left(1 - \left|\dfrac{x - x_{min}}{\Delta x}\right|\right), & x \in [x_{min} - \Delta x, x_{min} + \Delta x], \\ 0, & \text{elsewhere,} \end{cases} \tag{E 1}$$

with $H_{min} < 0$. This function can be Fourier-expanded as

$$H(x) = \frac{H_m \Delta x}{2\pi} + \frac{2}{\pi \Delta x} H_{min} \sum_{\substack{m=-\infty \\ m \neq 0}}^{m=+\infty} \frac{1}{m^2} \sin^2\left(\frac{m\Delta x}{2}\right) \exp[\mathrm{i}m(x - x_{min})], \tag{E 2}$$

and function $G$ defined by (5.8) can therefore be approximated as

$$G_{app}(\hat{\tau}) = \left(\frac{\hat{T}}{2\pi}\right)^{1/2} H_{min} \frac{4}{\pi \Delta x} F(x), \tag{E 3}$$

with

$$F(x) = \sum_{m=1}^{m=+\infty} \frac{1}{m^{5/2}} \sin^2\left(\frac{m\Delta x}{2}\right) \cos\left[m(x - x_{min}) - \frac{\pi}{4}\right], \tag{E 4}$$

which is (5.12). In order to obtain an estimate of the maximum of $F(x)$, we first reformulate it as:

$$F(x) = C(x) + S(x), \tag{E 5}$$

with

$$C(x) = \frac{1}{4\sqrt{2}} \sum_{m=1}^{+\infty} \frac{1}{m^{5/2}} [2\cos m(x - x_{min}) - \cos m(x - x_{min} + \Delta x) - \cos m(x - x_{min} - \Delta x)] \tag{E 6a}$$

$$S(x) = \frac{1}{4\sqrt{2}} \sum_{m=1}^{+\infty} \frac{1}{m^{5/2}} [2\sin m(x - x_{min}) - \sin m(x - x_{min} + \Delta x) - \sin m(x - x_{min} - \Delta x)]. \tag{E 6b}$$

Let us set:

$$Z(X) = \sum_{m=1}^{+\infty} m^{-1/2} (\cos mX + \sin mX). \tag{E 7}$$

It can be seen that, differentiating (E 5), (E 6) twice, $F''(x)$ is the sum of three series of the form (E 7):

$$F''(x) = \frac{1}{4\sqrt{2}} [Z(x - x_{min} - \Delta x) + Z(x - x_{min} + \Delta x) - 2Z(x - x_{min})]. \tag{E 8}$$

A theorem by Zygmund (1959) states that

$$\sum_{m=1}^{+\infty} m^{-\beta} \cos mX \underset{X \to 0}{\simeq} |X|^{\beta - 1} \Gamma(1 - \beta) \sin \pi \frac{\beta}{2}, \tag{E 9a}$$

$$\sum_{m=1}^{+\infty} m^{-\beta} \sin mX \underset{X \to 0}{\simeq} \mathrm{sgn}(X) |X|^{\beta - 1} \Gamma(1 - \beta) \cos \pi \frac{\beta}{2}, \tag{E 9b}$$

for any $\beta \in [0, 1[$. Therefore, taking $\beta = 1/2$, we obtain

$$Z(X) \underset{X \to 0}{\simeq} \mathscr{H}(X) |X|^{-1/2} \sqrt{2} \Gamma(1/2), \tag{E 10}$$

where $\mathscr{H}$ is the Heaviside function. For small enough $\Delta x$, any $x$ in the neighbourhood of $x_{min}$ is also in the neighbourhood of $x_{min} - \Delta x$ and $x_{min} + \Delta x$, so that, from (E 8), we can approximate $F''(x)$ as

$$F''(x) \simeq F''_{app}(x) = \frac{\Gamma(1/2)}{4}\left[\frac{\mathscr{H}(x - x_{min} - \Delta x)}{|x - x_{min} - \Delta x|^{1/2}} + \frac{\mathscr{H}(x - x_{min} + \Delta x)}{|x - x_{min} + \Delta x|^{1/2}} - 2\frac{\mathscr{H}(x - x_{min})}{|x - x_{min}|^{1/2}}\right]. \quad \text{(E 11)}$$

Integrating twice yields

$$F(x) \simeq F_{app}(x) = \frac{\Gamma(1/2)}{3}\left[f(x - x_{min} - \Delta x) + f(x - x_{min} + \Delta x) - 2f(x - x_{min})\right] + Ax + B, \quad \text{(E 12)}$$

where $f$ is defined by

$$f(X) = \mathscr{H}(X)\,|X|^{3/2},$$

and $A$, $B$ are two integration constants. Clearly, $A$ should be 0 to avoid a spurious discontinuity of $F$ at $x = 2n\pi$ and $B$ must be calculated so that the approximation of $F$ has a zero average on $[0, 2\pi]$, as does the original function (E 4). This condition yields

$$B = \frac{\Gamma(1/2)}{15\pi}\left[2(2\pi - x_{min})^{5/2} - (2\pi - x_{min} - \Delta x)^{5/2} - (2\pi - x_{min} + \Delta x)^{5/2}\right].$$

It can be easily checked that $F_{app}(x)$ has a maximum at $x = x_{min} + \Delta x/3$ whose value is

$$F^{max}_{app}(x) = \frac{2\Gamma(1/2)}{3\sqrt{3}}\Delta x^{3/2} + B. \quad \text{(E 13)}$$

Owing to the approximation used to obtain (E 11), it is clear that approximation (E 12) becomes better for smaller $\Delta x$. Figures 9(*a*) and 9(*b*) shows a comparison of the calculated series (E 4) (solid line) and its approximation by (E 12) (dashed line) for $x_{min} = \pi$ and $\Delta x = \pi/2$ (figure 9*a*) or $\Delta x = \pi/10$ (figure 9*b*). For $\Delta x$ as large as $\pi/2$ (in this case the peak spans over half of the interval), the maximum of $F$ is still predicted with a relative error as low as 8 %. For $\Delta x = \pi/10$, it is reduced to 1.25 %. Moreover, it can be noted that the approximation of $F$ is good not only near $x_{min}$, where it should be, but also over the whole interval $[0, 2\pi]$.

The quality of the approximation of $\max_x F$ can be seen in figure 9(*c*), in which the relative error $\epsilon = |F^{max} - F^{max}_{app}|/F^{max}$ is displayed as a function of $\Delta x$: since for a typical inertial bubble, $\Delta x$ amounts to $10^{-9}$, it is clear that the approximation given by (E 13) is excellent. We also draw the value of the constant $B$ relative to $F^{max}_{app}$ on figure 9(*d*), which shows clearly that $B$ can easily be neglected for $\Delta x$ smaller than $10^{-2}$.

Finally, it is of interest to know the characteristic relaxation time of function $F$ after it has reached its maximum. It can be shown after some algebra that $F$ reaches a fraction of its maximum value $\alpha F^{max}$ after a time approximately equal to $27\Delta x/64\alpha^2$. Applying this formula shows that $F$ is still equal to one fifth of its maximum value after $10.5\Delta x$, and to one tenth after $42\Delta x$.

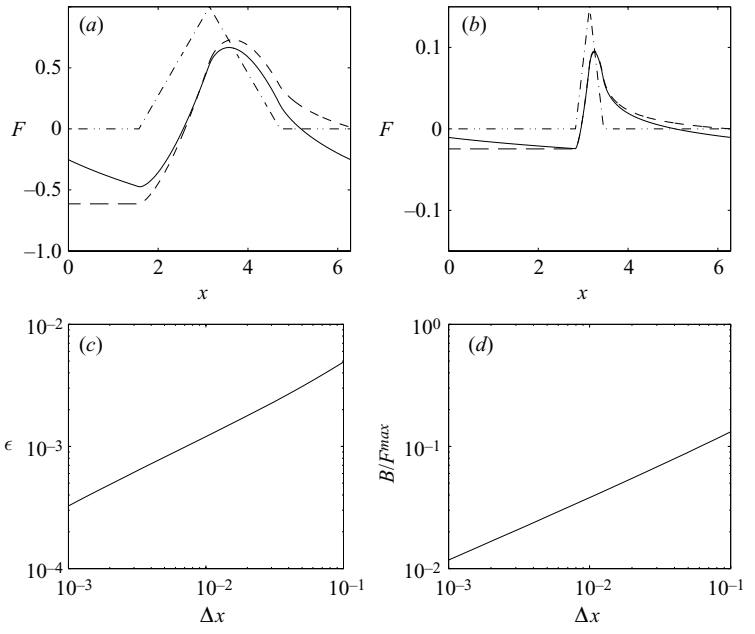


FIGURE 9. (*a*,*b*) Comparison of function $F$ calculated numerically from (E 4) (solid line) with function $F$ calculated by approximation (E 12) (dashed line). The dash-dotted line recalls the shape of the tooth approximation, (E 1), of function $H$. (*a*) $\Delta x = \pi/2$. (*b*) $\Delta x = \pi/10$. (*c*) Relative error on the maximum value of $F$ calculated from (E 12), as $\Delta x$ is varied. (*d*) Ratio $B/F^{max}$ as $\Delta x$ is varied.

## REFERENCES


AKHATOV, I., GUMEROV, N., OHL, C., PARLITZ, U. & LAUTERBORN, W. 1997 The role of surface tension in stable single bubble sonoluminescence. *Phys. Rev. Lett.* **78**, 227–230.

ARCHIBALD, W. J. 1938 The process of diffusion in a centrifugal field of force. *Phys. Rev.* **53**, 746–752.

BIRD, R. B., STEWART, W. E. & LIGHTFOOT, E. N. 1960 *Transport Phenomena*. John Wiley.

BRENNER, M. P., HILGENFELDT, S. & LOHSE, D. 2002 Single-bubble sonoluminescence. *Rev. Mod. Phys.* **74**, 425–483.

CRUM, L. A., MASON, T. J., REISSE, J. L. & SUSLICK, K. S., (ed.) 1999 *Sonochemistry and Sonoluminescence*, *Proc. NATO Advanced Study Institute on Sonoluminescence and Sonoluminescence, Leavenworth, Washington, USA, 18–29 August 1997*, Kluwer.

ELLER, A. & FLYNN, H. G. 1965 Rectified diffusion during nonlinear pulsations of cavitation bubbles. *J. Acoust. Soc. Am.* **37**, 493–503.

FUJIKAWA, S. & AKAMATSU, T. 1980 Effects of the nonequilibrium condensation of vapour on the pressure wave produced by the collapse of a bubble in a liquid. *J. Fluid Mech.* **97**, 481–512.

FYRILLAS, M. M. & SZERI, A. J. 1994 Dissolution or growth of soluble spherical oscillating bubbles. *J. Fluid Mech.* **277**, 381–407.

FYRILLAS, M. M. & SZERI, A. J. 1995 Dissolution or growth of soluble spherical oscillating bubbles: the effect of surfactants. *J. Fluid Mech.* **289**, 295–314.

FYRILLAS, M. M. & SZERI, A. J. 1996 Surfactant dynamics and rectified diffusion of microbubbles. *J. Fluid Mech.* **311**, 361–378.

HICKLING, R. & PLESSET, M. S. 1964 Collapse and rebound of a spherical bubble in water. *Phys. Fluids* **7**, 7–14.

HILGENFELDT, S., LOHSE, D. & BRENNER, M. P. 1996 Phase diagrams for sonoluminescing bubbles. *Phys. Fluids* **8** (11), 2808–2826.

HILGENFELDT, S., BRENNER, M. P., GROSSMAN, S. & LOHSE, D. 1998 Analysis of Rayleigh-Plesset dynamics for sonoluminescing bubbles. *J. Fluid Mech.* **365**, 171–204.

Hirschfelder, J. O., Curtiss, C. F. & Bird, R. B. 1967 *Molecular Theory of Gases and Liquids*. John Wiley.

Hsieh, D. Y. & Plesset, M. S. 1961 Theory of rectified diffusion of mass into gas bubbles. *J. Acoust. Soc. Am.* **33**, 206–215.

Kaschiev, D. 2000 *Nucleation : Basic Theory with Applications*. Butterworth–Heinemann.

Keller, J. B. & Miksis, M. 1980 Bubble oscillations of large amplitude. *J. Acoust. Soc. Am.* **68**, 628–633.

Larson, M. A. & Garside, J. 1986 Solute clustering in supersaturated solutions. *Chem. Engng Sci.* **41**, 1285–1289.

Lin, H., Storey, B. D. & Szeri, A. J. 2002 Rayleigh–Taylor instability of violently collapsing bubbles. *Phys. Fluids* **14**, 2925–2928.

Louisnard, O. & Gomez, F. 2003 Growth by rectified diffusion of strongly acoustically forced gas bubbles in nearly saturated liquids. *Phys. Rev.* E **67** (036610), 1–12.

Lyczko, N., Espitalier, F., Louisnard, O. & Schwartzentruber, J. 2002 Effect of ultrasound on the induction time and the metastable zone widths of potassium sulphate. *Chem. Engng J.* **86**, 233–241.

Mullin, J. W. & Leci, C. L. 1969 Evidence of molecular cluster formation in supersaturated solutions of citric acid. *Phil. Mag.* **19** (161), 1075–1077.

Plesset, M. S. & Zwick, S. A. 1952 A nonsteady heat diffusion problem with spherical symmetry. *J. Appl. Phys.* **23**, 95–98.

Prosperetti, A. 1999 Old-fashioned bubble dynamics. In *Sonochemistry and Sonoluminescence* (ed. L. A. Crum, T. J. Mason, J. L. Reisse & K. S. Suslick), *Proc. NATO Advanced Study Institute on Sonoluminescence and Sonoluminescence, Leavenworth, Washington, USA, 18–29 August 1997*, Kluwer.

Prosperetti, A. & Lezzi, A. 1986 Bubble dynamics in a compressible liquid. Part 1. First-order theory. *J. Fluid Mech.* **168**, 457–478.

Storey, B. D. & Szeri, A. 2000 Water vapour, sonoluminescence and sonochemistry. *Proc. R. Soc. Lond.* A **456**, 1685–1709.

Storey, B. D. & Szeri, A. 2001 A reduced model of cavitation physics for use in sonochemistry. *Proc. R. Soc. Lond.* A **457**, 1685–1700.

Storey, B. D. & Szeri, A. J. 1999 Mixture segregation within sonoluminescence bubbles. *J. Fluid Mech.* **396**, 203–221.

Toegel, R., Gompf, B., Pecha, R. & Lohse, D. 2000 Does water vapor prevent upscaling sonoluminescence? *Phys. Rev. Lett.* **85**, 3165–3168.

Tomita, Y. & Shima, A. 1977 On the behaviour of a spherical bubble and the impulse pressure in a viscous compressible liquid. *Bull. JSME* **20**, 1453–1460.

Zygmund, A. 1959 *Trigonometric Series*. Cambridge University Press.